ENDOCHRONIC CONSTITUTIVE MODELING OF MARINE FIBER REINFORCED CONCRETE AND FROZEN SOIL

By

RAJA K. GOPAL

A DISSERTATION PRESENTED TO THE GRADUATE SCHOOL
OF THE UNIVERSITY OF FLORIDA IN
PARTIAL FULFILLMENT OF THE REQUIREMENTS
FOR THE DEGREE OF DOCTOR OF PHILOSOPHY

UNIVERSITY OF FLORIDA

1985

ACKNOWLEDGEMENTS

The author would like to express his sincere gratitude to his supervisor, Dr. D.V. Reddy, Professor of Ocean Engineering, Florida Atlantic University, for his guidance, encouragement, and availability throughout this investigation. He is grateful to Dr. H. Wang, Professor and Chairman of Coastal and Oceanographic Engineering, for serving as the Chairman of the supervisory committee and for providing the financial support for part of this work. Thanks are due to Drs. M.A. Eisenberg and C.T. Sun, Professors in the Department of Engineering Sciences and Dr. F.E. Fagundo, Assistant Professor of Civil Engineering, for serving as members of the supervisory committee and for their comments and criticisms.

He would like to thank Dr. S.E. Dunn, Professor and Chairman, Department of Ocean Engineering, Florida Atlantic University, for making his stay possible at Ocean Engineering Department, Florida Atlantic University, to continue the dissertation work under the supervision of Dr. D.V. Reddy. The financial support from Florida Sea Grant College, Dr. D.V. Reddy's Grant Nos. R/C-7 and R/C-D-10, is gratefully acknowledged.

Special thanks are due to the computer centers at the University of Florida and Florida Atlantic University. The

facilities for stress-strain testing provided by Jammal & Associates at their West Palm Beach Laboratory and the help rendered by Mr. G.G. Nomikos and D.T. Thiel in carrying out various tests are gratefully acknowledged. Experimental data on frozen soil provided by Dr. V.R. Parameswaran, National Research Council, Ottawa, Canada is highly appreciated. Many thanks are due to Dr. S. Smith, Assistant Professor of Ocean Engineering, Florida Atlantic University, for permitting the author to print the first draft of this dissertation on his printer.

He would like to thank his parents and other family members for their constant encouragement to pursue higher higher education. Finally, he would like to acknowledge all his friends, in particular Mr. T. Sashidhar, M.M. Kunjapur, W.C. Wang, S. Ioardanis, and L. Chin-Loi, for their warm friendship which made these four years very joyous.

TABLE OF CONTENTS

LIST OF TABLES

LIST OF FIGURES

Abstract of Dissertation Presented to the Graduate School of the University of Florida in Partial Fulfillment of the Requirements for the Degree of Doctor of Philosophy

ENDOCHRONIC CONSTITUTIVE MODELING OF MARINE FIBER REINFORCED CONCRETE AND FROZEN SOIL

By

Raja K. Gopal

August 1985

Chairman: H. Wang
Cochairman: D.V. Reddy
Major Department: Engineering Mechanics

This dissertation describes the application of endochronic (endos=internal, chronos=time) theory, which is a unified viscoplastic theory, to the analysis of fiber reinforced concrete structures subjected to marine exposure. Endochronic analysis has opened up new avenues of constitutive modeling enabling a realistic analysis of structures taking into account material nonlinearities. Unlike the conventional plasticity-based theories, this formulation does not need the definition of a yield surface; instead it uses the concept of an intrinsic time defined in terms of both strain and time to analyze elastic as well as plastic behavior in a continuous manner. The theory has been successfully used to analyze metals, soils, and concrete.

The experimental data are obtained by testing fiber reinforced concrete specimens subjected to varying periods

of circulating sea water exposure. Uniaxial compressive stress-strain behavior is determined by testing concrete cylindrical specimens in parallel with a co-axial special alloy heat treated steel tube. The endochronic constants defining the material behavior are found by using an optimization procedure based on the experimental stress-strain behavior. Experimentally determined flexural behavior is predicted based on the endochronic constants and a probabilistic method to account for the tensile contribution of fibers intersecting a unit cross sectional area. The agreement between the experimental and predicted behavior is very encouraging.

The presentation includes a description of the behavior of concrete in the marine environment, the properties of fiber reinforced concrete, and recent improvements in the endochronic formulation, such as plastic strain and jump kinematic hardening formulations, which overcome the earlier deficiencies like the open hysteresis loops under cyclic loading. A simplified extension of the endochronic formulation is presented to analyze the thermally sensitive materials like ice and frozen soil. This formulation is used in conjunction with a finite element analysis program to analyze the response of a typical Arctic offshore island foundation. The numerical procedures used are described in the Appendix.

CHAPTER I
INTRODUCTION

1.1 General Introduction

This dissertation is an analytical and experimental study of fiber reinforced concrete exposed to the marine environment and frozen soil. An endochronic (endos= internal, chronos=time) theory, a unified viscoplastic theory, is used to analytically predict the experimental flexural behavior. The endochronic formulation has been extended by including the thermal and creep effects to analyze the response of a typical Arctic offshore island foundation.

Concrete is generally considered to be an ideal marine construction material, requiring little or no maintenance, due to its inertness in sea water. Good concrete with a low permeability, submerged in sea water, increases in strength with the passage of time. Concrete has been used in the past for marine structures like breakwaters and sea walls, and even in ship building. With the increase in offshore oil exploration activity, concrete is assuming an increased role in offshore construction. Concrete gravity platforms are very well adapted for the severe environmental areas like the North Sea and Arctic regions. Because of the long lasting

nature of concrete in sea water, nuclear industry is considering the use of thick concrete shells for marine disposal of nuclear wastes.

In spite of its high compressive strength, concrete has low tensile strength. This is the major factor in the initiation of cracks and deterioration of many reinforced concrete structures in the marine environment. When the reinforcing steel corrodes, the resulting oxide products occupy larger volumes giving rise to internal tensile stresses. Once the concrete cracks, the corrosion mechanism accelerates due to the easier access of the corroding medium to the embedded steel. This phenomenon has lead to the deterioration of many coastal structures. The cost of replacement and repair of bridge structures alone in the U.S.A. is projected to be around 6.3 billion dollars. Some of the methods used to prevent the cracking from the embedded metal corrosion are i) use of high strength concrete with larger clear cover, ii) use of epoxy coated steel reinforcement, iii) chemical inhibitors, and iv) cathodic protection. High strength concrete has a lesser porosity affording a greater immunity to the steel from the corroding medium. Research is being done on the use of epoxy coatings for steel, and some corrosion inhibitors like calcium nitrate in the concrete mix for retarding or preventing steel corrosion.

1.2 Special Concretes

Recently, many techniques have been developed to improve the tensile behavior of concrete. One effective but expensive method is to reduce the internal flaws by filling the pores with polymeric substances. There are three different types of polymer concretes:

1) Polymer-Impregnated Concrete (PIC): The capillary pores in the hardened concrete are impregnated by a liquid monomer which is subsequently polymerized to form the solid polymer insitu within the pores.

2) Polymer Concrete (PC): Consists of a mix of aggregate and polymer with no cement. The polymer acts as the binder for the aggregate.

3) Latex-Modified Concrete (LMC): Polymer latex, a colloidal suspension of polymer in water, is added to the concrete mix at the mixing stage.

All the methods produce hard, dense, and high strength concrete. Some of the applications of polymer concretes have been in the overlays for pavements and in the construction of seafloor spherical hull structures for oil storage.

Another way of improving the tensile behavior of concrete is by adding short, discontinuous fibers which restrict the crack growth by bridging across them. The fibers make the concrete behave like a pseudo-ductile material instead of its usual brittle behavior. They have been used to reinforce brittle materials since ancient times;

straw was used to reinforce sunbaked bricks even during the Biblical periods, and more recently, asbestos fibers have been used to reinforce portland cement. Fiber reinforced concrete has been applied in many instances where the performance of ordinary concrete was unsatisfactory. Steel fiber reinforced concrete was found to reduce the thickness of airport runways by one half. It has been used in the successful repair of stilling basins of dams damaged by floating debris digging through the ordinary concrete linings. Another successful application was for the linings in hydraulic structures where cavitation was a big problem. Steel fiber reinforced dolosse units were found to survive severe winter storms during which time corresponding ordinary concrete units suffered extensive damage. Polypropylene fibers are widely used for concrete piles, in view of their excellent impact resistance properties. Glass fibers have been indicated as a substitute for the hazardous asbestos fibers. Typical marine application of fiber reinforced concrete is that for breakwater armor units.

1.3 Constitutive Modeling Techniques

In the analysis of concrete structures, concrete has been modeled as a linear elastic, ideally plastic, or work-hardening plastic material. In view of the highly nonlinear behavior of concrete, all the above methods are only approximations. Linear elastic modeling is reasonable only at low stress levels; for high stress levels plastic formu-

lations become necessary. These theories, originally developed for metals and later adapted for concrete, assume the existence of a yield criterion coupled with a hardening rule to define the subsequent yield surfaces. There is no uniqueness associated with the choice of yield surfaces leading to an ambiguity in the results. These models can be viewed as discontinuous-material models, as the material response is separately analyzed in various stages i.e., loading, unloading, and reloading. However, real material behavior is usually continuous and includes many complicated cross effects. Very often, such discontinuous models, instead of simplifying the problem, are the sources of numerical difficulties and inefficiences.

On the other hand, the recently developed endochronic theory describes the material behavior in a continuous manner without the need of a yield surface definition. This overcomes the uncertainties associated with the choice of yield surface. This theory describes the behavior in terms of an intrinsic time function, which is a non-decreasing scalar variable that depends on the increments of both strain and time. The intrinsic time parameter represents the extent of change or damage of the internal structure of a material subjected to deformation. This seems to be one of the most comprehensive theories, capable of modeling strain hardening, softening, unloading and reloading, cross hardening and other nonlinear features of concrete.

1.4 Outline of the Dissertation

Chapter II reviews the literature in the areas of marine concrete, fiber reinforced concrete, and the constitutive theories to model its behavior. The discussion includes the causes for the deterioration of concrete structures in the marine environment, improvements in the concrete properties due to the fiber addition, various past and present constitutive modeling theories, and the techniques for the analysis of concrete structures. Chapter III discusses the adaptation of endochronic theory to model various nonlinear features of concrete. The experimental techniques to obtain the complete stress-strain curves and the determination of endochronic constants are also presented. The development of an analytical model to predict the load-deflection behavior of fiber reinforced concrete beams is discussed in Chapter IV. The analytically predicted behavior is compared with that obtained by experimental methods. Chapter V presents an extension of the endochronic formulation to include the thermal sensitivity of materials like ice and frozen soils. This formulation is used in conjunction with a finite element analysis program to analyze the foundation response of a typical Arctic offshore island composed of frozen soil. Chapter VI concludes the dissertation with some suggestions for further work in this area. Various numerical techniques used in the investigation are discussed in Appendix-A.

CHAPTER II
LITERATURE REVIEW

This chapter reviews the literature on four different aspects covering the entire dissertation as follows:

1) Durability of concrete in sea water,

2) Fiber reinforced concrete,

3) Constitutive models for concrete,

and

4) Flexural analysis of concrete beams.

2.1 Durability of Concrete in Sea Water

There are basically three corrosion zones in a marine structure: immersed, splash and tidal, and atmospheric as shown in Fig. 2.1. The basic mechanism of deterioration of concrete in any zone is due to an internal expansion of either the concrete or reinforcing steel. In addition, the structural elements are subjected to different environmental and biological effects depending on the vertical location.

Marine concrete structures can fail due to the deterioration of the reinforcing steel or the concrete itself. Magnesium salts dissolved in the sea water can deteriorate the concrete without the corrosion of steel reinforcement. Sulphates, present in the sea water mostly as magnesium

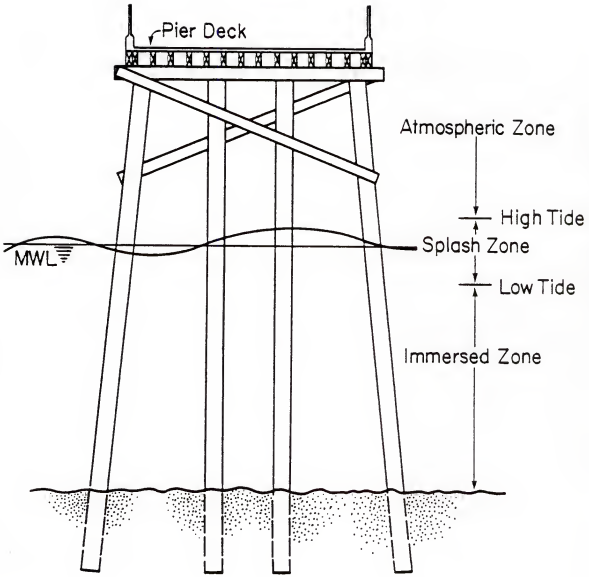

Fig. 2.1 Corrosion Zones in an Offshore Concrete Structure

salts, react with tricalcium aluminate (C_3A) in the cement paste to form sulphoaluminate hydrate (ettringite), which has more than twice the volume of C_3A, leading to a swelling of concrete and cracking. A proper choice of cement with low C_3A contents, low water-cement ratio, and air entrainment reduces the damage due to this kind of corrosion. In the normal marine environment this effect is negligible compared to the effect due to reinforcement corrosion.

When the steel corrodes, its corrosion products occupy a considerably larger volume, typically two to three times the original volume of metal before corrosion. As a result, high internal tensile stresses are created which can disrupt the surrounding concrete and cause cracks to form. Reduced cross sectional areas of steel may also lead to structural failures, being more critical with the prestressing steel tendons than with larger reinforcing bars. The alkalinity of cement in concrete is usually adequate to provide the required pH level to make the steel passive to corrosion. However, over a period of time chlorides in the sea water penetrate the concrete and depassivate the steel, making it corrode even when the surrounding concrete is alkaline. Another mechanism of steel corrosion is due to the non-uniformities in the chemical composition and the resultant electric potentials. Supply of oxygen is essential for this mechanism to function. Houston and Ferguson (1972) reported that the ratio of clear cover to

bar diameter should exceed three, to provide a reasonable protection to steel.

In the immersed zone the structural members are acted upon by marine organisms and fouling elements like barnacles. They increase the surface area and the roughness, attracting greater forces on the structure. They could also cause local corrosion and differential aeration cells due to the pockets of entrapped oxygen. A hard, dense concrete with a smooth surface is said to reduce the chances of this kind of a damage.

In the splash and tidal zones, the additional corrosion mechanisms are due to alternate wetting and drying from tide cycles, wear and abrasion, and a localized pitting due to cavitation. Alternate wetting and drying may cause cracks due to the resulting volume changes. Evaporated sea water usually leaves behind its salt contents which can accelerate the corrosion. Again, a hard, dense concrete is reported to reduce the damage in this zone.

Corrosion in the atmospheric zone is mainly due to the salt-laden humid atmosphere above the sea surface. If the concrete is permeable the chlorides in the atmosphere reach the steel reinforcement in the concrete and promote corrosion. Another mechanism, though rare in marine environment, can be due to the reaction of carbon dioxide in the atmosphere with the hydroxides in the concrete. This reaction, referred to as carbonation, reduces the alkalinity of concrete to such a level where the passivity is destroyed

and corrosion can start. Additional details on the corrosion mechanisms of concrete in sea water have been discussed by Beeby (1978), Mather (1982), Schupak (1982), and Taylor and Sharp (1978).

Field studies to determine the durability of concrete have been carried out by O'Neil (1980). Reinforced concrete beams, with and without air entrainment, were exposed to natural weathering conditions at Treat Island, Maine, for over twenty years. The effect of various concrete mix parameters on the durability of concrete was evaluated. Similar studies have also been carried out by Gjorv (1971) in Norway. The nature of the two investigations requires a long duration of time to evaluate the durability of concrete.

Nishibayashi, Yamura, and Inoue (1980) described an accelerated test procedure to evaluate the durability of concrete in sea water. Concrete mixes with different types of cement, water-cement ratios, and curing histories were subjected to cycles of immersion in sea water for 24 hours followed by an oven drying at 60 to 80^{o}C. In addition to visual observation for cracks, the reduction in dynamic modulus of elasticity and length changes were made every ten cycles for 200 cycles. By comparing the extent of damage and other physical characterestics to the findings of Gjorv (1971), they concluded that 200 cycles of accelerated testing corresponds to a 30-year exposure in the marine environment, i.e., each cycle is equivalent to 50 to 60 days of actual field exposure. Similar techniques were

employed by Reddy, Gopal, Nomikos, and Thiel (1984) to evaluate the durability of marine fiber reinforced concrete.

A numerical method to predict the corrosion rates of reinforcement and the time required for the first crack formation was proposed by Bazant (1979a). Various features included in the model are transport of oxygen and chloride ion through the concrete cover, mass sinks and sources of oxygen, ferrous hydroxide and hydrated rust due to chemical reactions, depassivation of steel due to critical chloride ion concentration, cathodic and anodic potential due to concentration polymerization of electrodes, and flow of electric current through the electrolyte in the concrete pores. Practical applications of the model were described in the second part of Bazant's paper (1979b).

2.2 Fiber Reinforced Concrete

The basis for the concepts of fiber reinforced concrete was provided by the early research of Romualdi and Batson (1963a), and Romualdi and Mandel (1964) on the effects of the closely spaced reinforcing wires on the tensile strength of concrete. They found that for the same volume of reinforcing steel, the tensile strength of concrete is significantly increased, if the spacing between the wires is reduced to less than 10.2 mm (0.4 in.). This finding can be explained from Griffith's fracture theory which states that the tensile strength is inversely related to the length of the critical flaws, with an inherent assumption that the

critical flaws are of the same dimension as wire spacing. It was observed that the results of the closely spaced continuous wires could be achieved by mixing short lengths of fibers directly in the concrete.

The concrete properties have been improved to such an extent by the addition of fibers that many applications of it are foreseen which were considered to be impractical before. The increasing attention the fiber reinforced concrete has been receiving is reflected by more than 2,000 references reported by Hoff, Fontenot, and Tom (1976) and Hoff (1977,1979). ACI Committee 544 (1973) has published a State-of-the art report on fiber reinforced concrete. The guidelines for measuring the properties of fiber reinforced concrete have been discussed by ACI Committee 544 (1978). In this section some of the aspects of fiber reinforced concrete are briefly reviewed.

2.2.1 Various kinds of fibers

Fiber reinforced concrete is a composite material consisting of cement-based matrix and an ordered or randomly distributed short fibers. Many different kinds of fibers have been developed for use in concrete. Fiber types can be divided into two main groups: those with moduli higher than the cement matrix, such as steel, glass, asbestos, and those with moduli lower than the cement matrix, such as nylon, polypropylene, and kevlar. Steel, glass, kevlar, and polypropylene are the most frequently used fibers. Due to the

health hazards, the use of asbestos fibers has been discontinued recently.

Steel fibers are usually of the straight type. But to improve the bond special types like hooked-end, crimped, and Duoform have been developed. Though steel fibers have high strengths and are found to produce stiff composites, they only increase the first crack strength marginally. If the composite is designed to fail by fiber fracture, they increase the ultimate strength considerably. Some of the applications of these fibers have been as overlays for roads, pavements, bridge decks, airport run ways, and industrial flooring. Due to their susceptibility to corrosion, further studies are needed for their application to offshore environments.

Glass fiber reinforced concrete is being considered as a substitute for, and improvement of asbestos fibers. The major problems are fiber breakage due to instability and the surface degradation by the high alkalinity of the hydrated cement paste. While alkali resistant (AR) fibers are more stable than ordinary E-glass fibers, the degree and severity of time-dependent strength degradation and their performance in wet conditions are still subject to speculation. One of the important property improvements obtained by glass fiber inclusion is the spectacular increase in the impact strength compared to asbestos fibers. The use of high alumina cement and pulverized fuel ash in the matrix can improve the durability of these fibers.

Both polypropylene and kevlar fibers belong to the class of plastic fibers. They have high tensile strengths, but their low-moduli precludes reinforcing effects. However, their high elongation capacity (15-25 percent), makes them absorb large amounts of energy, enabling the composite to absorb 10 to 25 times more impact energy than the plain mortar or concrete. The most extensive use of polypropylene fibers is in concrete piles. The superior impact resistance properties of these fibers is due to a purely mechanical bond between the fiber and concrete. Though kevlar fibers have not been used in the concrete, their future applications seem to be promising due to their similarity to polypropylene fibers.

2.2.2 Suitability to the marine environment

Though fiber reinforced concrete has many superior structural properties than plain concrete, its suitability to marine applications will depend on the stability of the fibers in a marine environment. Only a few of the many publications on fiber reinforced concrete pertain to its marine applications.

Barab and Hansen (1973) described the performance of steel fiber reinforced breakwater armor units. After one winter of exposure to ocean storms, the steel fiber units were found to have no damage, whereas some of the similar non-fiber units placed at the same time sustained some cracking. Fiber reinforced units showed superior impact

resistance compared to the ordinary units. Due to the limited duration of marine exposure, no comments were made regarding durability.

Based on their tests on metal fibers, Rider and Heidersbach (1980) recommended stainless steel fibers for marine applications. Concrete beam specimens with three different types of steel fibers, stainless, carbon, and meltex (melt-spun stainless) were exposed to circulating sea water for up to 12 months. Flexural strengths were determined as an indication of the fiber durability. No evidence of corrosion-induced damage was evident on any of the stainless steel fibers examined by electron microscope, whereas the other types had traces of corrosion.

Reddy, Gopal, Nomikos, and Thiel (1984) studied the strength and durability of marine exposed concrete reinforced with three different kinds of fibers, steel, glass, and kevlar with and without latex modification. Compressive, tensile, flexural, and impact strengths were measured at various periods of sea water exposure as an indication of structural integrity. Long term durability was studied with alternate exposure to sea water and oven drying. Kevlar fibers were found to be more stable than the steel and glass fibers. The addition of latex was found to significantly improve the durability characteristics.

2.2.3 Mechanics of fiber action

The fibers act as crack arrestors that restrict the growth of flaws in the matrix, controlling them from enlarging under stress into cracks which eventually cause failure. This process considerably increases the static and dynamic properties of concrete, its toughness, ductility, and impact resistance. The major factors which control the performance of the composite are the relative fiber-matrix stiffness, volume content and other physical factors of fibers, and the fiber-matrix interfacial bond.

Relative stiffness

For an efficient stress transfer to the matrix, the elastic modulus of fibers should be much higher than that of the matrix. Based on simple volume proportions, the composite cracking strength in static tension was obtained by Hannant (1976) as:

$$\sigma_{cu} = \sigma_{mu} [\, 1 + V_f(M - 1) \,] \qquad (2.2.1)$$

σ_{cu} = cracking strength of composite,

σ_{mu} = cracking strength of matrix,

V_f = volume percentage of fibers,

and

$$M = \text{modular ratio} = \frac{E_{fiber}}{E_{matrix}}$$

It can be easily seen from Eq. 2.2.1 that only high modulus fibers with high 'M' values can bring about an improvement in the strength of the composite. Low modulus fibers with

'M' less than unity decreases the strength. High strength, high modulus fibers impart characteristics of strength and stiffness to the composite. Low modulus, high elongation fibers are capable of large energy absorption characteristics, and impart a greater degree of toughness and resistance to impact and explosive loading. The former also contributes to these dynamic properties but to a lesser extent.

Critical volume percent

Based on the properties of fibers and matrix in the composite, a critical volume percentage, $V_{f(crit)}$, can be found which will enable the fibers to carry the load the composite sustains before cracking. By satisfying the force equilibrium before and after the fracture, the critical volume percentage can be expressed as follows in the form given by Hannant (1976):

$$V_{f(crit)} = \frac{\sigma_{mu}}{(\sigma_{fu} - \varepsilon_{mu}E_f + \sigma_{mu})} \qquad (2.2.2)$$

where

σ_{mu} = ultimate cracking strength of matrix,

σ_{fu} = ultimate fracture strength of fibers,

ε_{mu} = fracture strain of matrix,

and

E_f = elastic modulus of fiber.

If the volume content of fibers exceeds the $V_{f(crit)}$, the failure is usually by debonding which results in multiple cracking of concrete. This is a desirable situation because

it changes a basically brittle material with a single fracture surface and low energy requirement to fracture into a pseudo-ductile material that can absorb transient minor overloads and shocks with little visible damage.

Interfacial bond

The fiber-matrix interfacial bond plays an important role in the post-fracture behavior of composites. High bond strengths are required for improved tensile resistance but a lower interfacial bonding would improve the fracture toughness and impact resistance through energy dissipation and damping at the interfacial discontinuities. If the interfacial bond is such that the composite failure occurs by pull-out, then the matrix becomes the principal tensile load carrying element, with only a modest increase in tensile strength. To achieve a truly two-phase composite action, the matrix must be so designed as to transfer load to the fibers so that they contribute fully to the composite strength. The fiber physical parameters, length and diameter, can be so chosen that the failure of composite would be by fiber fracture, when the full bond strength is developed over one quarter of the length, i.e., $\frac{\ell}{4}$. For this to happen, the bond force developed should be higher than the load required for fiber fracture, i.e.,

$$\tau \pi d \frac{\ell}{4} \geq \frac{\pi}{4} d^2 \sigma_{fu} \qquad (2.2.3)$$

or,

$$\frac{\ell}{d} \geq \frac{\sigma_{fu}}{\tau} \qquad (2.2.4)$$

Hence, a suitable aspect ratio can be chosen for the fibers depending upon the requirements. The ultimate composite strength for the case of a failure by fiber pull-out is

$$\sigma_{cu} = N \tau \frac{\ell}{d} \qquad (2.2.5)$$

and, for the case of fiber fracture,

$$\sigma_{cu} = N \sigma_{fu} \qquad (2.2.6)$$

where N is the number of fibers intersecting a unit cross-sectional area. For random fiber distribution, 'N' is obtained by probabilistic methods, discussed in the sub-section 2.2.4

Other factors

The above discussion, and the equations are only valid for the most ideal case, when the fibers are aligned in the load direction and the full bond strength is developed as found by pulling tests on a single fiber. If the fibers are aligned randomly, some correction factors have to be applied, which will considerably reduce the theoretical strength. Actual fiber bond strengths are less than the ones found in the pulling tests, due to the fiber-fiber interaction. An analogy to this interpretation is the decrease of the total bearing capacity of a group of foundation piles when the piles are brought closer to each other.

Zollo (1975) described extrusion techniques which enable the most favorable fiber orientation and bond

characteristics. Naaman and Shah (1976) described the pull-out mechanism in steel fiber reinforced concrete. They observed that the peak pull-out load of a single fiber is much higher compared to that of a group of fibers. The mechanics of fiber reinforcement has been discussed by Shah and Rangan (1971), Swamy, Mangat, and Rao (1973), Swamy (1974), Hannant (1978). McKee (1969) has presented equations for the fiber spacing in terms of the fiber diameter and the volume content.

2.2.4 Probabilistic analysis techniques

As the Eqs. 2.5 and 2.6 indicate, the theoretical strength of the random fiber composites depends on the probabilistic number of fibers intersecting a unit cross-sectional area. Some of the probabilistic models are discussed in this section.

Matsuishi and Iwata (1982) studied the probabilistic strength of steel fiber reinforced concrete. The expected value of mean strength, with and without considering the fiber pull-out effects, was obtained as a product of the probability of fibers intersecting the cross section and the load carried by the fibers. For the case with fiber pull-out effects, a separate function which depends on the fiber lengths was constructed. The probabilistic number of fibers per unit area of the composite for the random fiber distribution is as follows:

$$N = \frac{2V_f}{\pi d^2} \tag{2.2.7}$$

The major limitation of the study was the non-inclusion of fiber interaction effects in the strength calculations.

Naaman, Moavenzadeh, and McGarry (1974) assumed a Poisson distribution for the statistical distribution of the fibers in the concrete mass. The tensile member was assumed to be made up of a chain of a series of N consecutive links, breaking at the weakest link. It was assumed that the failure mode after matrix cracking is ductile. The analytical model predicts the casual effects of given dominant parameters, e.g. the volume fraction and the aspect ratio of fibers, the bond and tensile strength of matrix on the composite strength, derived either from the data or from the assumptions on which the model is based. The fiber interaction effects were considered in the model. The following relations were derived for the number of fibers, bond-strength, and the composite cracking and ultimate strengths for a one link chain member:

$$N = \frac{2V_f}{\pi d^2} \tag{2.2.8}$$

$$\bar{\tau} = \tau - 0.52\ N, \tag{2.2.9}$$

$$\sigma_{cc} = \sigma_{mu}\ (1 - V_f) + \alpha\bar{\tau}\frac{\ell}{d}V_f, \tag{2.2.10}$$

$$\sigma_{cu} = \frac{1}{\pi}\bar{\tau}V_f\frac{\ell}{d} < \sigma_{fu}V_f, \tag{2.2.11}$$

and

$$\text{variance}(\sigma_{cu}) = \frac{\pi}{A}V_f\bar{\tau}^2\ell^2\ \left(\frac{1}{8} - \frac{1}{3\pi^2}\right), \tag{2.2.12}$$

where

σ_{cc} = average composite cracking strength,

σ_{cu} = average composite post-cracking strength,

α = a constant determined experimentally,

A = cross-sectional area of the link,

τ = average bond strength determined from pull-out test on a single fiber,

and

$\bar{\tau}$ = reduced bond strength due to fiber interaction effects.

Eq. 2.2.9 for the fiber interaction effects was found by curve fitting the experimental results on 0.254 mm(0.01 in.)- diameter fibers.

2.2.5 Models for fiber behavior

Shah and Rangan (1971) considered a two-phase composite materials approach to develop the stress-strain curve of the composite incrementally by using secant modulus and Poission's ratio of the two components at different strain levels, i.e., based on the properties of concrete and fibers at different strain levels, the composite properties are determined at the corresponding strain levels. The secant modulus for the random fiber concrete is written as:

$$E_{RC} = \sqrt{E_{90} E_0} \qquad (2.2.13)$$

where

E_{90} = secant modulus with transversely aligned fibers,

and

E_0 = secant modulus with longitudinally aligned fibers.

The expressions used for E_{90} and E_0 as proposed by Tsai (1964) and Hansen (1965) are rather complicated. The stress is given by:

$$\sigma_{RC} = E_{RC}\, \varepsilon_C \qquad (2.2.14)$$

By repeating the process at different strain levels, the complete stress-strain curve for the composite is developed.

Tanigawa and Hatanaka (1983) developed mathematical expressions for the hysteretic-strain behavior of steel fiber reinforced concrete under repeated compression. They observed that the envelope equation developed by Popovics (1973) for plain concrete is valid even for the steel fiber reinforced concrete. Different expressions were developed for loading, unloading, and reloading portions of the hysteresis curve in terms of volume content and aspect ratio of fibers.

Keer (1981) developed general equations based on the ACK (Aveston, Cooper, and Kelly) theory (1971), to describe the loading, unloading, and reloading behavior of a cracked fiber cement composite. In particular, the theoretical relationships between the unloading strain and the resulting residual strain at zero load and subsequent reloading modulus were examined. This formulation would be useful in analyzing the fiber composites subjected to a short term overload or overstrain sufficient to crack it.

Stroeven (1982) developed constitutive relations for a cracked region of a composite based on morphological observations. The stress transfer capability of a cracked region in plain or fiber reinforced concrete was analyzed in terms of the micromechanical aspects of the particle interlock mechanism.

2.2.6 Fracture mechanics methods

The concepts of fiber reinforced concrete originated with the application of linear elastic fracture methods by Romualdi and Batson (1963b) to find that the strength of concrete in tension is limited by internal holes and microcracks. It was found that the tensile cracking strength of concrete increases in proportion to the inverse square root of the reinforcing bar spacing. Since that time fracture mechanics has been applied to many fiber composite analyses.

Hillerborg, Modeer, and Petersson (1976) developed a method in which fracture mechanics methods are introduced into finite element analysis by means of a model where stresses are assumed to act across a crack as long as it is narrowly opened. The crack is assumed to propagate when the stress near the crack tip reaches the tensile strength. When the crack opens, the stresses are not assumed to fall to zero at once, but to decrease with the increasing crack width. The analytical and experimental strengths of both

reinforced and unreinforced beams were found to compare well.

The suitability of the J-integral as a fracture criterion for fiber reinforced concrete has been studied by Mindess, Lawrence, and Kesler (1977). The J-integral is a path-independent energy line integral, a one parameter average measure of the elastic-plastic field near a crack tip. It can be considered as the potential energy difference between two identically loaded beams having differing crack lengths, which may be interpreted as the energy available for crack extension. By testing notched beams with differing amounts of glass and steel fibers in bending, the J-integral parameter K_{IC} (critical stress intensity factor) and G_{IC} (critical strain energy release rate) were evaluated. J_{IC} was found to be a superior indicator of the effectiveness of fiber addition than the other parameters.

A similar study carried out by Velazco, Visalvanich, and Shah (1980) concluded that the R-curve, a plot of stress intensity factors against the corresponding crack lengths, is more promising than the other methods. Various fracture mechanics methods studied include critical stress intensity factor, J-integral, critical crack opening displacement, compliance techniques for determining the slow crack growth, and R-curve analysis. They tried to identify a fracture parameter, independent of test specimen geometry, which can correctly predict the effects of fiber addition, and concluded that the R-curve approach is the most promising.

This approach was also found to be satisfactory by Wecharatana and Shah (1983).

2.3 Constitutive Models for Concrete

This section focuses on various past and present constitutive models used in the analysis of concrete. The newly developed endochronic theory is evaluated with respect to the conventional plasticity theories. Recent advances in the endochronic theory are briefly summarized.

Due to the lack of proper experimental data, concrete structures have been analyzed in the past on the basis of linear elastic-fracture models. Though these are attractive in terms of their simplicity and required computational efforts, they are accurate up to a small fraction of the failure loads and result in conservative designs. Recent experimental work on complete stress-strain curves in both uniaxial and more complex loading conditions has enabled the development of curve-fitting and nonlinear elastic methods. Equivalent uniaxial models have been formulated for biaxial and triaxial loading conditions. Also, perfect and work-hardening plasticity theories were developed expressing plastic strains in terms of assumed yield surfaces. These models predict different plastic behavior for different yield surfaces. To overcome the ambiguity associated with the choice of yield surface in the plastic theories, endochronic i.e., unified viscoplastic theories, have been developed. Excellent

summaries of various methods have been presented by Nilsson (1979), Chen and Ting (1980), and Chen (1982). These methods can be catogerized into various groups as follows:

1) curve-fitting methods,

2) linear and nonlinear elastic theories,

3) perfect and work-hardening theories,

4) visco-elastic and visco-plastic theories,

and

5) endochronic theories.

2.3.1 Curve-fitting methods

Based on the analysis of experimental data, many stress-strain relations were proposed in terms of the maximum principal stress and the corresponding strain. Popovics (1970, 1973), Darwin and Pecknold (1977), and Wang, Shah, and Naaman (1978a) discussed various curve fitting functions such as polynomials, exponential, fractional and statistical functions. Popovics (1970) discussed a numerical approach to describe the complete stress-strain curve in terms of the maximum compressive stress and the corresponding strain. This was later verified by the same investigator (1973) based on large experimental data.

A rational approach was proposed by Wang, Shah, and Naaman (1978a). Separate functions were constructed for the ascending and descending portions, in terms of four constants which were determined from four conditions that the curve passes through the origin, the peak, a specified point

after the peak, and the curve has a specified secant modulus at 45 percent of the compressive strength. A similar method was proposed by Sargin (1971) in terms of a parabolic curve.

All the above models are limited to uniaxial cases only. A widely used formula, proposed by Liu, Nilson, and Slate (1972), valid for both uniaxial and biaxial cases, has the following form:

$$\sigma = \frac{a\varepsilon}{1 + \left(a\frac{\varepsilon_p}{\sigma_p} - 2\right)\left(\frac{\varepsilon}{\varepsilon_p}\right) + \left(\frac{\varepsilon}{\varepsilon_p}\right)^2} \qquad (2.3.1)$$

where

σ, ε = stress and strain in the principal stress direction,

σ_p, ε_p = experimentally determined values of maximum principal stress and the corresponding strain,

and

a = initial tangent modulus in uniaxial loading.

For the case of biaxial loading, 'a' is defined as:

$$a = \frac{E}{(1 - \nu\alpha)} \qquad (2.3.2)$$

in which

α = ratio of the principal stress in the orthogonal direction to that in the direction considered,

and

ν = Poisson's ratio in uniaxial loading.

The basic concept is to treat the biaxial stress-strain behavior of concrete as an equivalent uniaxial relationship. The strain increment in each principal direction

is evaluated solely by the principal stress in that direction and the corresponding tangent stiffness. Poisson's ratio is assumed to be constant. This model has the disadvantage that it is applicable only to certain simple structural elements, like beams and panels, and cannot model the hydrostatic pressure sensitivity or the volume increase near failure.

2.3.2 Linear elastic models

In these models, linear elastic relations in terms of E and ν are used to model both uncracked and cracked behavior. If a principal stress exceeds the tensile strength of concrete, a crack is assumed to form and the concrete is modeled as an orthotropic material. Stress in the normal direction to crack is redistributed to the adjacent members in the structure. When the compressive strain exceeds a prescribed value, concrete is assumed to be crushed, loosing its strength completely. Some applications of linear elastic models have been discussed by Ngo and Scordelis (1967), and Suidan and Schnobrich (1973).

2.3.3 Nonlinear elastic models

In linear elastic models, the elastic moduli G and K are assumed constant. But this is unrealistic in view of the nonlinearity of concrete. In nonlinear elastic models, they are expressed as functions of stresses or strains, usually in terms of octahedral components. Depending on the

way stresses and strains are related, the nonlinear models are classified into three different types: Cauchy, Hyperelastic, and Hypoelastic. In the Cauchy type formulation, the current state of stress is expressed as a function of current state of deformation as follows:

$$\sigma_{ij} = F_{ij}(\epsilon_{kl}) \tag{2.3.3}$$

This formulation does not depend on the history of stress or strain, and may lead to a positive energy creation.

Hyperelastic (Green) type are based on the assumption of the existence of a strain energy-density function W, such that

$$\sigma_{ij} = \frac{\partial W}{\partial \epsilon_{ij}} \tag{2.3.4}$$

in which W is a function of the current components of stress and strain tensors, defined as:

$$W = \int_0^{\epsilon_{ij}} \sigma_{ij}\, d\epsilon_{ij} \tag{2.3.5}$$

This ensures that no energy can be generated through load cycles, and laws of thermodynamics are always satisfied.

Hypoelastic formulations, also called incremental formulations, are used to describe the material behavior in which the state of stress depends on the current state of strain as well as on the stress path followed to reach that state. The incremental constitutive relations for time-independent materials are written as:

$$\dot{\sigma}_{ij} = F_{ij}\,(\,\dot{\epsilon}_{kl},\, \sigma_{mn}) \tag{2.3.6}$$

in which $\bar{\sigma}_{ij}$ and $\bar{\varepsilon}_{kl}$ are the stress and strain increment tensors, and σ_{mn} are the current stress tensor components.

Recently, incremental stress-strain relations have been formulated for a special class of hypoelastic materials in which the function 'F' is assumed to depend on the stress (or strain) tensor itself. Murray (1979) has summarized these models in a comprehensive manner. Gerstle (1981a and 1981b) presented simple formulations for biaxial and triaxial behavior in terms of variable bulk and shear moduli. Kupfer and Gerstle (1973), and Darwin and Pecknold (1977) presented incremental biaxial stress-strain relations for concrete in terms of variable tangent moduli and Poisson ratio.

2.3.4 Perfectly plastic models

Under multiaxial stress cases, especially under triaxial compression, concrete was observed to flow like a ductile material on the yield or failure surface before reaching the crushing strain. Plastic or irrecoverable strains are assumed to take place once the yield surface is reached; they are obtained from the normality conditions. The complete stress-strain relationships are developed in three parts: 1) before the yield, 2) during plastic flow, and 3) after fracture. The total strain is expressed as a sum of elastic and plastic parts as follows:

$$d\varepsilon_{ij} = d\varepsilon^{e}_{ij} + d\varepsilon^{p}_{ij} \qquad (2.3.7)$$

The elastic strains are determined from Hooke's law or any nonlinear elastic model

$$d\varepsilon^{e}_{ij} = C_{ijkl}\, d\sigma_{kl} \tag{2.3.8}$$

in which C_{ijkl} is an elastic modulus tensor, and $d\sigma_{ij}$ is the stress increment tensor. The plastic strain increment is written as follows:

$$d\varepsilon^{p}_{ij} = d\lambda \frac{\partial g}{\partial \sigma_{ij}} \tag{2.3.9}$$

in which $g(\sigma_{ij})$ is called the plastic potential surface, usually taken as the yield surface, f. This gives an associated flow rule

$$d\varepsilon^{p}_{ij} = d\lambda \frac{\partial f}{\partial \sigma_{ij}} \tag{2.3.10}$$

in which $d\lambda$ is a positive scalar factor of proportionality that is nonzero only when plastic deformations occur.

Some of the yield surfaces considered by previous researchers include: 1) the Von-Mises criterion, 2) Extended Von-Mises criterion (or Drucker-Prager criterion), and 3) Coulomb or modified Coulomb criterion.

2.3.5 Work-hardening plasticity models

The most recent of the plasticity theories are the strain-hardening or work-hardening formulations. These theories are developed to account for the experimental observation that, after a limited plastic flow, the materials harden requiring higher stresses to cause further

straining. A yield surface, termed a loading surface, combining both perfect plasticity and strain-hardening, is postulated and an associated flow rule is used for the plastic strains before fracture.

According to this approach, the stresses under operating conditions are expected to be in the initial discontinuous range such that the concrete behavior can be characterized as linear elastic. This initial discontinuous surface is the limiting surface for elastic behavior. When the material is stressed beyond the elastic limit surface, a subsequent new discontinuous surface called the loading surface is developed, which replaces the initial elastic surface. If the material is unloaded from and reloaded within this subsequent loading surface, no additional irrecoverable deformation will occur until this new surface is reached. If straining is continued beyond this surface, further discontinuities and additional irrecoverable deformations result. Three different kinds of hardening rules are commonly used: isotropic, kinematic, and mixed.

Bazant (1977) discussed the numerical stability of the plasticity theories used in finite element analysis. Rudnicki and Rice (1975) proposed an incremental plastic theory which exhibits inelastic dilatancy, sensitivity to hydrostatic pressure, and internal friction. Plasticity theories have been reviewed in considerable detail in a recent book by Chen (1982).

2.3.6 Viscoelastic and viscoplastic models

None of the plasticity based formulations can model the time-dependent or strain rate-dependent behavior. Various viscoelastic and viscoplastic models have been developed to take these two effects into account. Viscoelastic models have been applied to model the creep and age-dependent behavior of concrete by Bazant (1975).

2.3.7 Endochronic models

In plasticity theories, plastic or irrecoverable strains are assumed to form after the yielding takes place. But in reality they may occur right from the beginning due to internal grain rearrangement like in soil or concrete, which is not accounted for in the plasticity theories. Another limitation of plasticity theories is that there is a certain ambiguity associated with the choice of a proper yield surface. Loading and unloading criteria, needed to determine the plastic strains, cause unnecessary complications in the numerical computations.

The endochronic theory proposed by Valanis (1971) overcomes some of the limitations of plasticity formulations. The theory, derived on the basis of irreversible thermodynamics, has been applied to predict the mechanical response of metals under complex strain histories. Jain (1982), provided an excellent summary of the thermodynamic derivation of the endochronic constitutive equations.

The basic concept underlying the endochronic formulations is the characterization of the material strain state in terms of an intrinsic time, which is a non-decreasing scalar variable that depends on the increments of strain as well as time, and geometrically represents the length of the path traced by the states of the material in a strain-time space of suitable metric, i.e., the memory of the material is expressed in terms of an intrinsic parameter. The early versions of the theory were rate-independent; time was not involved in the intrinsic time terms. The distance along a strain path between two strain states P and P' in Fig. 2.2, denoted as $d\zeta$, termed the intrinsic time measure, is defined as follows:

$$d\zeta^2 = P_{ijkl}\, d\epsilon_{ij}\, d\epsilon_{kl} \qquad (2.3.11)$$

The tensor P_{ijkl} is a material property tensor as it varies from material to material. The stress at point 'P' is not determined simply by the strain at 'P', but by the history of the strain along the path OP. Valanis termed the materials for which the stress is a function of the strain history with respect to an intrinsic time scale, as endochronic (Greek: endo=inner, chronos=time), and the corresponding theory as endochronic theory.

To account for the experimental observation that the materials strain harden, the intrinsic time scale Z is defined as follows:

$$dZ = \frac{d\zeta}{f(\zeta)} \; ; \quad \frac{dZ}{d\zeta} > 0; \; Z \geq 0 \qquad (2.3.12)$$

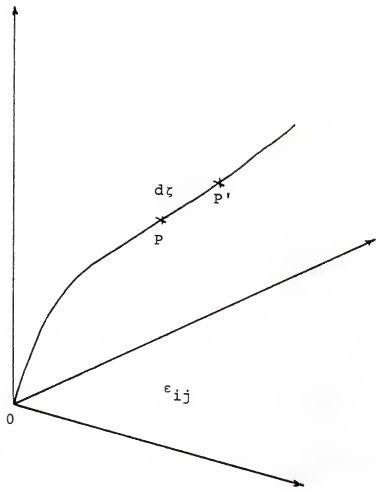

Fig. 2.2 Path in Strain Space

in which $f(\zeta)$ is a monotonically increasing material property-dependent hardening function. The intrinsic time scale Z is representative of the deformation history of the material. The basic stress-strain relations of Valanis are presented below:

If the temperature effects are neglected, Eqs. 3.24 and 3.25 of Valanis (1971) can be simplified to a form:

$$\sigma_{ij} = 2 \int_0^Z \mu(Z - Z') \frac{\partial \varepsilon_{ij}}{\partial Z'} dZ' \qquad (2.3.13)$$

Considering a single exponential term for the modulus,

$$\mu(Z) = \mu_0 e^{-\alpha Z} \qquad (2.3.14)$$

then

$$\sigma_{ij} = 2 \mu_0 \int_0^Z e^{-\alpha(Z-Z')} \, d\varepsilon_{ij}(Z'), \qquad (2.3.15)$$

in which $$d\varepsilon_{ij} = \frac{\partial \varepsilon_{ij}}{\partial Z'} dZ' \qquad (2.3.16)$$

Integrating Eq. 2.3.15 following the Leibnitz rule, results in

$$d\varepsilon_{ij} = \frac{d\sigma_{ij}}{2\mu_0} + \frac{\alpha}{2\mu_0} dZ \, \sigma_{ij} \qquad (2.3.17)$$

The first term on the right in the above equation resembles the classical elastic term and the second term that of plastic term. The form of the above equation recognizes the experimental observation that plastic strains can occur immediately following the loading. The plastic strain term in Eq. 2.3.17,

$$d\varepsilon_{ij}^{p} = \left(\frac{\alpha}{2\mu_0} dZ \right) \sigma_{ij} \qquad (2.3.18)$$

is similar to the Prandtl-Reuss relation of classical plasticity

$$d\varepsilon^{p}_{ij} = (d\lambda)\sigma_{ij} \qquad (2.3.19)$$

Endochronic theory contains these relations of classical plasticity as a special case. But this formulation is continuous and 'dZ', does not depend on any postulations or inequalities. On the contrary, $d\lambda$ needs the postulation of a yield surface and the loading and unloading criteria.

Recent applications

Endochronic theory was first applied to concrete by Bazant and Bhat (1976) by extending the formulation for metals developed by Valanis (1971) to include many nonlinear features of concrete like hydrostatic pressure sensitivity, inelastic dilatancy due to deviatoric strains, strain hardening, and softening. The model was able to predict stress-strain diagrams for concrete of different strengths, failure envelopes of uniaxial, biaxial, and triaxial stress-strain diagrams, lateral strains and volume expansion, hysteresis loops for repeated compression, strain rate effects, and creep behavior. This is the only constitutive theory which can model all the above nonlinear features of concrete at the present time. Various endochronic constants were determined by fitting large sets of experimental data. It was indicated that those constants would be the same for any normal weight concrete with compressive strengths in the

range of 3500 to 6000 psi. The hysteretic behavior of concrete beams was predicted by Bazant and Bhat (1977) using the above model. The same formulation was applied to predict the finite element behavior of cubes, beams, and other concrete structural elements by Sorensen, Arnesen, and Bergan (1977).

Endochronic theory has also been extensively applied to soils. Bazant and Krizek (1976) proposed an endochronic model for the liquefaction of sand. This formulation was applied by Ansal, Krizek, and Bazant (1982) to predict seismic response of earth dams. Wu and Wang (1983) used an endochronic theory to predict the behavior of sand under static loading and Wu and Sheu (1983) described a method to model shear hysteresis behavior of sand. Bazant, Ansal, and Krizek (1982), and Valanis and Read (1982) discussed various applications of endochronic theory to soils. Gopal and Reddy (1985), and Reddy and Gopal (1985) applied endochronic theory to analyze the frozen soil behavior to a static loading in the Arctic offshore region.

Recent improvements

Although capable of modeling many complex phenomena, early endochronic formulations were unable to properly characterize the response to small cyclic stress oscillations superimposed on large static stresses. Those formulations do not predict a positive energy dissipation or closed hysteresis loops, and yield a reloading path that is

less steep than the unloading slope for small load-unload oscillations. Sandler (1978) and Rivlin (1981) pointed out that these theories implied a physically impossible condition of positive energy creation violating the Drucker stability postulate. It was indicated that this feature may lead to unstable solutions in wave propagation problems. Valanis (1981) has addressed some of these criticisms. Details of those criticisms are not discussed here as both of them were directed on the early formulations. Instead, the latter formulations, which overcome the deficiencies of earlier models, are discussed.

Plastic strain formulations

Valanis (1980) redefined intrinsic time in terms of plastic strains, instead of the total strain, which enables the formation of closed hysteresis loops. With this new definition, $d\zeta$ in Eq. 2.3.11 is rewritten as

$$d\zeta^2 = P_{ijkl}\, d\varepsilon^p_{ij}\, d\varepsilon^p_{kl} \qquad (2.3.20)$$

in terms of the plastic strain increments. It was established for the one-dimensional case that the rate of dissipation at the onset of loading, unloading, and reloading is zero, leading to closed hysteresis loops. The new model implies the existence of a yield surface in an 'a priori' fashion. Various versions of classical plasticity theories were shown to be particular cases of the endochronic formulation. This model was applied by Valanis and Read (1982) to

describe the soil response to cyclic shear loading, hydrostatic compression, and densification under cyclic shear. Lin and Wu (1983) applied the new endochronic formulation to obtain the cyclic behavior and plastic strain wave propagation in titanium alloys. Some of the recent developments of the endochronic theory and their applications were discussed by Valanis and Lee (1982). More recently, Valanis and Lee (1984) proposed an endochronic theory of cyclic plasticity which predicts very closely the experimental behavior of mild steel and grade 60 steel under various loadings.

Jump-kinematic hardening formulation

Bazant (1978) introduced the concept of 'jump-kinematic hardening' in endochronic theory to obtain closed hysteresis loops that ensure positive energy dissipation. The concept of a yield surface with a moving center was used. The basic definitions of inelastic deviatoric and volumetric strain increments were modified to include the hardening coefficients. In the original paper by Bazant and Bhat (1976) they were defined as follows:

$$de''_{ij} = \frac{s_{ij}}{2G}\, dZ \qquad (2.3.21)$$

and

$$d\varepsilon'' = d\lambda + \frac{\sigma}{3K}\, dZ' \qquad (2.3.22)$$

where

de''_{ij} , $d\varepsilon''$ = deviatoric and volumetric strain increments,

dZ, dZ' = intrinsic time increments,

$d\lambda$ = dilatancy parameter,

s_{ij} = deviatoric stress tensor,

and

σ = volumetric stress.

In the kinematic hardening model Eqs. 2.3.21 and 2.3.22 are modified as follows:

$$de''_{ij} = (s_{ij} - \alpha_{ij})\rho \frac{dZ}{2G} \tag{2.3.23}$$

and

$$d\varepsilon'' = d\lambda + (\sigma - \alpha)\psi \frac{dZ'}{3K} \tag{2.3.24}$$

in which

α_{ij}, α = current centers of the deviatoric and volumetric loading surfaces in stress space,

and

ρ, ψ = coefficients (less than unity) which reduce the rate of accumulation of inelastic strains in cases of unloading and reloading

ρ and ψ satisfy a certain inequality so as to assure closed hysteresis loops. For non-cyclic loading α_{ij} and α can be set to zero, and ρ and ψ to unity. For the case of cyclic loading, centers of the loading surface must jump into the extreme stress points whenever loading changes to unloading, or unloading to reloading. This can be explained as follows in reference to Fig. 2.3:

When the loading changes to unloading, the centers of the loading surfaces, α_{ij} and α, are moved to the extreme stress point in the loading path, i.e., to point 1. When the unloading is changed to reloading, the centers are moved to the extreme stress point in the unloading path, i.e.,

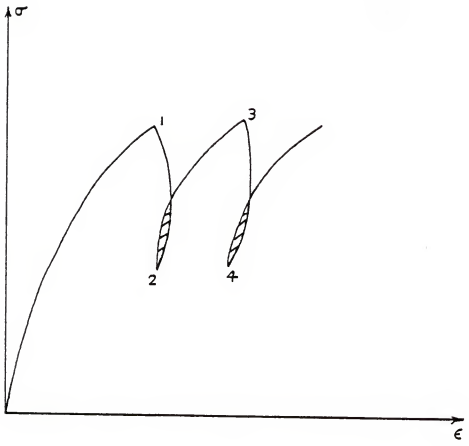

Fig. 2.3 Closed Hysteresis Loops in 'Jump-Kinematic' Hardening Model

point 2. Between the loading reversals they are kept constant. This process was found to give closed hysteresis loops even for an infinitesimal load-unload cases. More details on this formulation can be obtained from Bazant, Ansal, and Krizek (1982), and Bazant, Krizek, and Shieh (1983).

2.4 Flexural Analysis of Beams

2.4.1 Previous experimental investigations

Based on their experimental investigation, Shah and Rangan (1971), stated that 1.25 percent by volume of steel fibers increases the toughness of concrete (area under the load-deflection diagram), by as much as 20 times that for plain concrete. Relative toughness was found to increase with the aspect ratio (length to diameter ratio) of fibers. Snyder and Lankard (1972) discussed the factors affecting the flexural strength of steel fiber reinforced concrete. Fiber size limits were proposed for good workability.

Hughes and Fattuhi (1977a) discussed the effects of the addition of various fibers, including fibrillated and monofilament polypropylene, as well as round, straight, Duoform, crimped and hooked-end steel, upon the flexural properties of a basic concrete matrix at three different ages, 30, 90, and 190 days. The beams were tested at a constant central deflection of 0.029 mm per minute under third-point loading. Duoform steel fibers were found to be very effective due to their superior bond characteristics. This was

in contradistinction to crimped steel fibers that reduce the strength and toughness if present in large quantities, due to the shape-induced stress concentrations.

The present techniques of fibrous concrete flexural testing have been reviewed by Zollo (1980). Based on extensive testing with varying shear span to depth ratios, fiber and matrix types, it was concluded that testing of 4x4x 12 in. beams would be adequate to determine the flexural characteristics. Based on his experimental data, and comparable data from other sources, Johnston (1982) proposed a relationship which permits the flexural strength in any testing arrangement to be predicted from the values obtained in any other arrangement. A relationship was developed to predict the flexural strength in any testing arrangement, based on the strength of 6x6x18 in. specimens tested under third point loading.

2.4.2 Previous analytical investigations

Ngo and Scordelis (1967) were the first to apply finite element techniques to the analysis of concrete structures. They analyzed simply supported singly reinforced concrete beams for artificially introduced crack patterns using constant strain triangular elements. Concrete was modeled as a linear elastic material, and the bond between the steel and concrete was represented by bond-linkage elements.

Park, Kent, and Sampson (1972) analyzed the response of reinforced concrete members to cyclic loading. A layered beam element approach was used to obtain the load-deflection behavior of beams by an incremental method. For a given curvature increment at the mid-span section, the internal moment developed is found by an iterative procedure. This moment is prorated to different sections along the length of the beam and the corresponding curvatures are determined. Once the curvatures at all sections are found, the central deflection is obtained by integrating the curvature diagram. The same procedure was applied to the analysis of steel fiber reinforced concrete beams by Reddy and Gopal (1984).

Bazant and Bhat (1977) predicted the hysteretic behavior of reinforced concrete beams using the endochronic stress-strain formulation developed by them in 1976. They used the layered beam element approach as discussed before to formulate the section-equilibrium equations. Stiffness matrices of concrete and steel were assembled as discussed by Suidan and Schnobrich (1973). A perfect bond was assumed between steel and concrete. Finite element applications to concrete structures analysis have been discussed by Phillips and Zienkiewicz (1976), Valliappan and Doolan (1972), and Yuzugullu and Schnobrich (1973).

Rajagopalan, Parameswaran, and Ramaswamy (1974) proposed probabilistic equations for the ultimate moment carrying capacity of beams. Probabilistic coefficients were determined for various fiber alignments. Assuming a uniform

tensile stress distribution below the neutral axis, Hughes and Fattuhi (1977b) proposed equations for the flexural strength of cement based beams in terms of the aspect ratio, pull-out load for a single fiber, and the critical fiber length. These equations were found to compare well with the experimental strengths of steel and polypropylene fiber-reinforced concrete beams.

Parimi and Rao (1973) presented a method to calculate the fracture toughness of fiber-reinforced concrete, based on a realistic estimation of the spacing between randomly placed fibers. The analytical expressions, derived by energy methods, compared well with the experimental data on cement mortar and concrete specimens with steel fibers. Swamy and Mangat (1974) presented a combined crack arrest-composite materials theory to predict the first crack and ultimate flexural strength of steel fiber reinforced concrete beams. They assumed the fracture process to consist of two stages: initial stage, during which fibers debond with a slow crack propagation, and the final stage during which the failure occurs due to the unstable crack propagation when the fibers pull out and the interfacial shear stress reaches the ultimate bond strength. Wecharatana and Shah (1983) proposed nonlinear relations between the crack opening pressure and its opening. They divided the effective crack length into three zones: 1) a traction free zone, 2) a fiber bridging zone, and 3) a matrix process zone resulting from aggregate interlock and microcracking.

The crack closing pressure in the matrix process zone was assumed to be negligible, and ignored. The traction free zone is the one in which fibers are pulled out completely. Hence, only the fiber bridging zone offers resistance to the crack propagation. Analytical results from linear elastic fracture methods were found to compare well with the experimental data on notched beams.

Additional load-carrying capacity due to fibers

Additional moment carrying capacity of concrete beams due to steel fibers in the presence of the conventional steel reinforcement was discussed by Henager and Doherty (1976). The strength due to the fibers is directly added to that of the reinforcing bars to obtain the theoretical ultimate moment.

The recent trend in fiber reinforced concrete construction is to optimize the use of fibers to minimize the costs. Nagaraj and Dwarakanath (1984) proposed a method to estimate the capacity of partially fibrous concrete beams, in which the fibers are only provided in the tensile zone where they are active and no fibers are provided in compression zone where they are inactive. Their method is briefly discussed below.

The following assumptions were made:

1) the fibers are assumed to be uniformly distributed and randomly oriented,

2) flexural tensile stress σ_t, at which the ductile stress block builds up, is taken equal to the modulus of rupture of the plain concrete σ_m, i.e., $\sigma_t = \sigma_m$

3) strain in the composite corresponding to $\sigma_t = \sigma_m$ is considered identical to that of the matrix corresponding to its modulus of rupture

4) strain distribution across the depth of the section is linear

Fig. 2.4 shows the assumed stress and strain distribution across the depth of the section.

From the strain distribution diagram,

$$\frac{\varepsilon_{mut}}{\varepsilon_{cut}} = \frac{1}{t} = \frac{D - nD - kD}{D - kD} = 1 - \frac{n}{1 - k} \qquad (2.4.1)$$

i.e., $$n = \frac{(1 - k)(t - 1)}{t} \qquad (2.4.2)$$

where

ε_{cut} = ultimate strain of the matrix,

ε_{mut} = ultimate strain of the composite,

$t = \frac{\varepsilon_{cut}}{\varepsilon_{mut}}$ = tensile strain enhancement factor,

k = neutral axis depth factor,

and

n = height of the fibrous tensile zone to achieve a balanced failure.

Balanced failure is the failure at which the ultimate composite strain ε_{cut}, and the ultimate matrix strain, ε_{mut} will be reached simultaneously at the tensile extremity and the unreinforced concrete at the interface respectively.

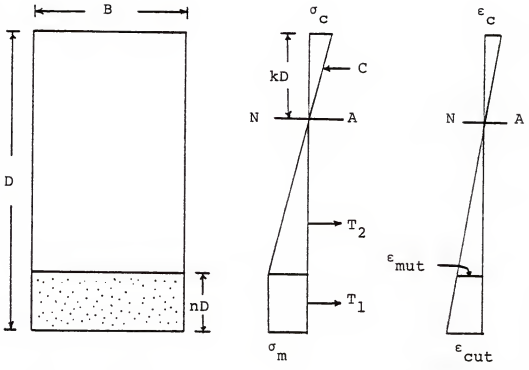

Fig. 2.4 Partially Fibrous Beam Section

From the stress distribution diagram, the equilibrium of the section can be written as follows:

$$\sigma_m \, n \, D + \frac{\sigma_m}{2} (1 - k - n)D = \frac{\sigma_c}{2} k \, D \qquad (2.4.3)$$

By solving Eq. 2.4.3, k can be written as

$$k = \frac{1 + n}{1 + r} \qquad (2.4.4)$$

in which

$$r = \frac{\sigma_c}{\sigma_t}$$

On substitution of 'n' from Eq. 2.4.2, k becomes

$$k = \frac{2 - \frac{1}{t}}{2 - \frac{1}{t} + r} \qquad (2.4.5)$$

The ultimate moment capacity can be computed as

$$M = T_1 [n \frac{D}{2} + (1 - k - n) D + \frac{2}{3} k D] + T_2 [\frac{2}{3} (1 - k - n) D + \frac{2}{3} k D] \qquad (2.4.6)$$

where

$$T_1 = \sigma_m B n D \qquad (2.4.7)$$

and

$$T_2 = \frac{1}{2} \sigma_m B (1 - k - n) D \qquad (2.4.8)$$

Substituting expressions for T_1 and T_2 in Eq. 2.4.6, and neglecting the second order terms in 'n', M can be written as:

$$M = \beta \sigma_m (\frac{BD^2}{6}) \qquad (2.4.9)$$

in which $\beta = 2 (1 + n - k)$, termed the moment capacity enhancement factor

The tensile strain enhancement factor, 't' is determined from a direct tension test on fiber concrete specimens. The analytical formulation was found to compare very well with the experimental results on steel fiber reinforced concrete beams with varying fiber contents.

CHAPTER III
ENDOCHRONIC STRESS-STRAIN MODEL FOR CONCRETE

3.1 Introduction

A complete stress-strain curve consists of an ascending part during which the stress in the specimen increases and a descending part during which the stress decreases; in both regions the strain continues to increase. A complete stress-strain curve is needed to predict nonlinear behavior accurately for extreme loading conditions, e.g., impact and earthquake loadings. The improvement in the concrete performance due to the fiber addition is reflected by the larger area under the stress-strain curve. After the concrete cracks, the fibers bridging the cracks provide resistance to the further crack growth and separation of concrete into fragments. Fiber reinforced concrete, therefore, behaves like a pseudo-ductile material, with higher stresses after the peak in unloading portion than the plain concrete.

When a concrete specimen is loaded in a conventional testing machine, both the specimen and the machine deform. When the stress in the specimen reaches a peak value, there is a reduction in the load which results in a sudden release of stored strain energy by the machine. This released strain

energy causes uncontrolled failure of the specimen. As a result, a stable descending part cannot be observed. In order to avoid uncontrolled failure, the load on the specimen must be reduced at a sufficiently fast rate to control the rate of strain energy release of the testing system.

3.2 Techniques for Obtaining Complete Stress-Strain Curves

There are basically two methods of obtaining a complete stress-strain curve. They are as follows:

1) use of a closed-loop testing system, and
2) in parallel-testing with a coaxial special alloy steel tube.

3.2.1 Closed loop testing system

In a closed loop testing system, any experimental output can be chosen and controlled as an independent variable. The experimental parameter is matched against its programmed counterpart. If a difference exists, an error signal is generated. This signal modifies the movement of the loading platen (cross head) according to the polarity and the magnitude of the signal so as to minimize it. For example, in a uniaxial compression test, the circumferential strain rate can be kept constant to obtain a stable descending part. The speed at which the testing system responds is an important factor in obtaining a stable descending portion of the curve. It depends on the frequency response or

the response time (electronic as well as hydraulic) of the system.

Hughes and Fattuhi (1977c) used this method to obtain the stress-strain behavior of fiber reinforced concrete cubes. A Losenhausen EHRI control unit, activated by three LVDT tranducers, was used to maintain a constant rate of deformation.

3.2.2 Testing with a steel tube in parallel

In this method concrete cylinders are loaded coaxially in parallel to a steel tube whose diameter is larger than that of the specimen. The tube is made of a heat treated special alloy, so that it displays a linear elastic behavior up to the desired maximum strain. It is so designed that the load on the system keeps on increasing even when the specimen is unloading. Load on the concrete specimen is determined using the strain and elastic modulus of steel tube. Strain in the concrete is assumed to be same as that in the steel tube.

This method offers an advantage over the other method in that the machine characteristics are not a determining factor in obtaining a stable descending portion of the curve. In spite of its simplicity it has certain limitations: the size of the concrete cylinder is limited to accommodate the additional load on the steel tube, and the failure of the specimen cannot be observed.

Wang, Shah, and Naaman (1978b) used this method to obtain complete stress-strain curves of normal and light-weight concrete in compression. Shah, Gokuz, and Ansari (1981) summarized various experimental techniques available for obtaining complete stress-strain curves.

3.3 Stress-Strain Relations

The endochronic formulation proposed by Bazant and Shieh (1978), used in this investigation, belongs to the family of theories with jump-kinematic hardening criteria, as described in Section 2.3. As the details of this formulation are discussed at considerable length by Bazant and Bhat (1976) and Bazant and Shieh (1978), only the salient points are presented here.

The deformations are assumed to be so rapid that the material is modeled as a rate-insensitive material by dropping the time-dependent intrinsic terms. The elastic properties are assumed to be incrementally isotropic and the stress-strain relations are written separately in terms of deviatoric and volumetric components as follows:

$$de_{ij} = de^{e}_{ij} + de^{p}_{ij} = \frac{ds_{ij}}{2G} + \frac{s_{ij}}{2G} dZ \qquad (3.1a)$$

$$d\varepsilon = d\varepsilon^{e} + d\varepsilon^{p} = \frac{d\sigma}{3K} + d\lambda + \frac{\sigma}{3K} dZ' + d\lambda' \qquad (3.1b)$$

where

$e_{ij} = \varepsilon_{ij} - \delta_{ij}\varepsilon$ = deviatoric components of the strain tensor,

$\varepsilon = \frac{1}{3}\varepsilon_{kk}$ = volumetric strain,

δ_{ij} = Kronecker delta,

$s_{ij} = \sigma_{ij} - \delta_{ij}\sigma$ = deviatoric components of the stress tensor σ

$\sigma = \frac{1}{3}\sigma_{kk}$ = volumetric stress,

K, G = bulk and shear moduli,

λ = inelastic dilatancy,

λ' = shear compaction,

and

Z, Z' = intrinsic times for distortion and compaction respectively.

The increments of intrinsic times are defined as follows:

$$dZ = \frac{d\zeta}{Z_1} \tag{3.2}$$

and

$$dZ' = \frac{d\zeta'}{Z_2} \tag{3.3}$$

where

$$d\zeta = \frac{d\eta}{f(\eta,\varepsilon,\sigma)} \; ; \; d\eta = F(\varepsilon,\sigma)d\xi$$

$$d\zeta' = \frac{d\eta'}{h(\eta')} \; ; \; d\eta' = H(\sigma)d\xi'$$

$$d\xi = \sqrt{J_2(d\varepsilon)} = \sqrt{\tfrac{1}{2}\, d\varepsilon_{ij}\, d\varepsilon_{ij}} \; ,$$

and

$$d\xi' = \sqrt{[\, I_1(d\varepsilon)\,]^2} = |\, d\varepsilon_{11} + d\varepsilon_{22} + d\varepsilon_{33}|$$

The increments of the inelastic dilatancy and shear compaction are defined as follows:

$$d\lambda = \ell(\lambda)\, L(\lambda, \varepsilon, \sigma)\, d\xi \qquad (3.4)$$

and

$$d\lambda' = \ell'(\lambda')\, L'(\lambda', \varepsilon, \sigma)\, d\xi \qquad (3.5)$$

where

J_2 = second invariant of the deviator of the tensor which follows in parentheses,

I_1 = first invariant of the tensor which follows in parentheses,

Z_1 , Z_2 = constants,

$f(\eta, \varepsilon, \sigma)$, $F(\varepsilon, \sigma)$ = distortion hardening and softening functions respectively,

$h(\eta')$, $H(\sigma)$ = compaction hardening and softening functions respectively,

$\ell(\lambda)$, $L(\lambda, \varepsilon, \sigma)$ = dilatancy hardening and softening functions respectively,

and

ξ, ξ' = non-decreasing scalar variables called distortion and compaction measure respectively.

3.3.1 Strain-hardening functions

Inelastic strain increments, whether due to plastic slip or due to microcracking, decrease as the residual strain increases. This is due to the fact that the potential locations of stress peaks gradually decrease with the accumulation of strain, which is evident more in the cyclic loading. As ζ and ζ' are adopted as the measures of the accumulated inelastic strain (or damage), function 'f' and 'h' must increase as ζ and ζ' increase. By analysis of test data,

the strain hardening functions were defined as follows by Bazant and Shieh (1978):

$$f(\eta,\varepsilon,\sigma) = \left(1 + \frac{\beta_1\eta + \beta_2\eta^2}{1 + F_2/a_7} \right) F_3 , \qquad (3.6)$$

$$F_3 = 1 + \frac{a_{10}}{J_2(\varepsilon)(1+a_9/\eta^2)} ,$$

and

$$h(\eta') = 1 + \frac{\eta'}{\beta_3} + \left(\frac{\eta'}{\beta_4} \right)^2 . \qquad (3.7)$$

In the above equations, F_3 is a function which makes the cyclic stress loops to contract more strongly at low cyclic deviatoric strains. Function F_2 governs the strain-softening behavior after the peak.

3.3.2 Strain-softening and hydrostatic pressure sensitivity

If the functions $F(\varepsilon,\sigma)$ and $H(\sigma)$ remain constant, the uniaxial stress-strain diagram would approach an asymptote of positive slope in which case the failure of the material will not be modeled. To obtain a gradual decrease of slope on approach to peak stress, the inelastic strain increments must be increased, obtained by an increase in F and H. Inelastic volume change due to hydrostatic pressure is taken into consideration through the intrinsic time

variable, ζ' called compaction measure. By analysis of test data the following softening functions have been found:

$$F(\varepsilon,\sigma) = F_1 + F_2 \tag{3.8}$$

where

$$F_1 = \frac{a_o(1-g_1)}{1-a_5(I_3^\sigma)^{1/3}\ (1+g_2)}$$

and

$$F_2 = \frac{a_2\ \sqrt{J_2(\varepsilon)}\ (1+|a_6 I_2^\sigma|^{1/4} + F_5)}{\{1 - a_1 I_1^\sigma + |a_8 I_2^\sigma|^{1/4} F_4 - a_3 I_3^\sigma\ (J_2(\sigma))^{1/8}\ (1+g_2)\}}$$

in which

$$g_1 = g_{11}\ g_{12},$$

$$g_2 = g_{21}\ g_{22}\ g_{23},$$

$$g_{12} = 1 - [\ 1 + (\ \frac{\sigma_{min}}{a_{17}(\sigma_{max} - a_{23})}\ )^4\ ]^{-1},$$

$$g_{11} = a_{14}\ [J_2\ (\varepsilon)]^{1/4}\ \frac{\sigma_{med}-\sigma_{min}}{\sigma_{max} - a_{23}}\ \{a_{15}(\frac{\sigma_{med}-\sigma_{min}}{\sigma_{max} - a_{23}})^{4/3} - a_{16}\},$$

$$g_{21} = \{\frac{a_{18}(\frac{\sigma_{med} - \sigma_{min}}{\sigma_{max} - a_{23}}) - 1}{a_{19}(1 - a_{20}\ \frac{|\sigma_{min}|}{\sigma_{max} - a_{23}})\ (\sigma_{min} - a_{23})}\ \}^{5/4},$$

$$g_{22} = [\ 1 + a_{21}\ (\ \frac{\sigma_{min}}{\sigma_{max} - a_{23}}\ )^4\ ]^{-1},$$

$$g_{23} = \left(\frac{\{J_2(\varepsilon)\}^{\frac{1}{4}}}{a_{22} + \{J_2(\varepsilon)\}^{\frac{1}{2}}} \right)^3 ,$$

$$F_4 = \left(\frac{\{J_2(\varepsilon)\}^{\frac{1}{4}}}{a_4 + \{J_2(\varepsilon)\}^{\frac{1}{2}}} \right)^3 ,$$

and

$$F_5 = a_{11}\sigma_{min}(1+a_{12}\sigma_{min})\left\{\frac{J_2(\varepsilon)^{\frac{1}{4}}}{|a_{13}\sigma_{min}|^{\frac{1}{4}} + \{J_2(\varepsilon)\}^{\frac{1}{2}}}\right\}^3$$

where

σ_{min}, σ_{med}, and σ_{max} are the minimum, medium, and maximum principal stresses. a_0 , a_1 , ... a_{22} are endochronic constants.

3.3.3 Dilatancy and compaction functions

The dilatancy functions govern the microcracking in the concrete. Since microcracking is primarily due to deviatoric strains, it is expressed as a function of $J_2(\varepsilon)$. The increments of the dilatancy parameter $d\lambda$, are given as follows:

$$d\lambda = \ell(\lambda)\, L(\lambda, \varepsilon, \sigma)\, d\xi \qquad (3.9)$$

where

$$\ell(\lambda) = 1 - \frac{\lambda}{\lambda_o}$$

and

$$L(\lambda, \varepsilon, \sigma) = \frac{c_3}{1 - c_1 I_1(\sigma)} \left\{ \left(\frac{\lambda}{\lambda_o}\right)^2 + \left(\frac{c_4 J_2(\varepsilon)}{c_2^2 + J_2(\varepsilon)} \right)^2 \right\}$$

Since the inelastic strains are due to the formation of microcracks, the incremental elastic moduli should decrease as the microcracking increases. The shear and bulk moduli G and K are expressed as follows:

$$G = \frac{1}{1 + c_5 \lambda} \frac{E_o}{2(1 + \nu)} \tag{3.10a}$$

and

$$K = \frac{1}{1 + c_5 \lambda} \frac{E_o}{3(1 - 2\nu)} \tag{3.10b}$$

In the above equations c_1, c_2 ... c_8 are endochronic constants and ν is the poisson ratio.

Inelastic strains due to hydrostatic pressure are modeled by a separate intrinsic term called shear compaction. It was assumed that the shear compaction will not have any effect on the moduli. The following functions are constructed:

$$\ell'(\lambda') = c_6 \left(1 - \frac{|\lambda'|}{\lambda'_o} \right)$$

$$L'(\lambda', \varepsilon, \sigma) = \frac{\sigma_{min}\, g_3^{1/3^o}}{1 + (g_3/c_8)^3}$$

and

$$g_3 = |c_7\, \sigma_{min}|^{0.93} - \sqrt{J_2(\varepsilon)}$$

in which c_6, c_7, and c_8 are the endochronic constants.

3.4 Experimental Investigation

3.4.1 Design of concrete mix

The design of a fiber reinforced concrete mix differs from that of the usual concrete in that, a special consideration is needed for the amount of cement in the mix and the size of the aggregate. ACI Committee 544 (1973), reported that a water cement ratio of 0.4 to 0.6, and a cement content of 3200 to 5530 N/c. m. (550 to 950 lb/c. yd.) are needed to ensure a sufficient quantity of cement paste to coat the fibers. To ensure a uniform dispersion of fibers, the aggregate size should not exceed 19 mm (0.75 in.) and preferably 9.5 mm (0.375 in.), Hannant (1978). The use of larger size aggregate may result in balling effects, where the fibers form clusters or balls resulting in a poor consistency of the mix. A maximum size lime rock aggregate of 9.5 mm (0.375 in.) corresponding to No. 89 stone was chosen to ensure good workability and uniform fiber distribution. Steel fibers of diameter 0.51 mm (0.02 in.), length of 30.5 mm (1.2 in.), and 0.5 percent by volume were used in the mix. The fibers were of the type "Dramix", ZP 30/50, with hooked ends collated in bundles with water soluble glue, manufactured by Bekaert Steel Wire Corporation. After the addition of fibers to the concrete mix, the glue dissolves separating the fibers which then disperse throughout the mix. The following mix proportions were chosen, based on the guidelines of Portland Cement Association (PCA)

published in 1979, which gives a 28 day compressive strength of 31 MPa (4500 psi).

Table 3.1
Mix Proportions of Concrete

Item	Content
water	2270 N/c. m. (390 lb/c. yd.)
cement	4950 N/c. m. (850 lb/c. yd.)
coarse aggregate	6170 N/c. m. (1060 lb/c. yd.)
fine aggregate	8420 N/c. m. (1447 lb/c. yd.)
super plasticizer	1750 cc/c.m. (59.5 fl. oz./c.yd.)
steel fibers	0.5 percent by volume

3.4.2 Fabrication of specimens

Fiber concrete specimens of diameter 76.2 mm (3 in.) and length 152.4 mm (6 in.) were cast in cardboard molds in three layers with external vibration and internal tamping with a thin rod. The rod used was thin enough not to disturb the fiber orientation. The specimens were removed from the molds after 24 hours, and cured for about a week with water sprinkling. They were then subjected to circulating sea water exposure of varying durations.

3.4.3 Alloy steel for coaxial loading jacket

A heat treated special alloy tube was used to encase the concrete cylinders for the stress-strain testing. The

jacket is of SAE 4140 grade steel, heat-treated to a Brinnel hardness of 445. The chemical composition of the alloy is given as follows:

Table 3.2
Chemical Composition of Alloy

Item	% volume	Item	% volume
carbon	0.38 - 0.43	manganese	0.75 - 1.0
phosphorus	0.04	sulphur	0.04
silicon	0.20 - 0.25	nickel	0.01
chromium	0.80 - 1.10	molybdenum	0.15 - 0.25

3.4.4 Test procedure

Complete stress-strain curves were obtained by testing the concrete specimens in parallel with a coaxial steel tube. One end of concrete cylinder was capped with sulphur capping material, according to ASTM C-617 standards. The concrete cylinder was then placed inside the steel tube and capped with hydrostone at the other end, to make it flush with the top of the steel tube. Fig. 3.1 shows the schematic diagram of the load sharing mechanism. A foil type strain gage of 350 ohms resistance, 0.5 inch length was fixed at each end of the diameter at mid-section of the steel tube. The strains were measured using a quarter bridge circuit in a Vishay digital strain indicator, Model P - 350A.

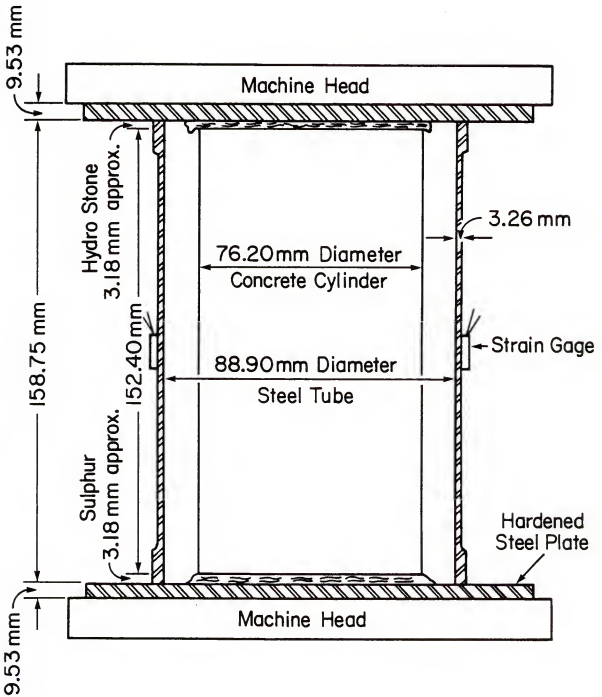

Fig. 3.1 Load Sharing Mechanism

The tests were carried out in a Forney hydraulic testing machine of capacity 1335 kN (300 kips). Fig. 3.2 shows the experimental set-up with the steel tube in the machine and the strain gage connections. The rate of straining was 10 micro-strains per second, which corresponds to approximately 30 psi per second on the concrete cylinder. This rate lies within the loading rates of 20 - 50 psi per second, recommended by ASTM C-39 standards for compressive strength testing of concrete cylinders.

3.5 Determination of Endochronic Constants

Various constants involved in the hardening, softening, and dilatancy functions of the stress-strain relations were found by curve-fitting the experimental behavior. At first, the values of the constants were varied manually to obtain a curve as close to the experimental one as possible. Then, an IMSL (International Mathematical and Statistical Library) subroutine "ZXSSQ", was used to minimize the sum of the squares of deviations between the experimental and predicted curve. The subroutine gives a local minimum of the sum of squares of M real functions in R real variables by using a finite difference Levenberg-Marquardt algorithm. The ordinates at various strain values were used as the real functions. The global minimum was obtained by repeating the optimization process with the new constants found in the previous iteration.

Fig. 3.2 Experimental Set-up for the Stress-Strain Tests

3.6 Results and Discussion

Figs. 3.3 and 3.4 show the stress-strain curves obtained for the plain and the steel fiber reinforced concretes at various periods of sea water exposure. The advantage of testing with a steel tube is evident by the controlled crack pattern shown in Fig. 3.5, in contrast to the crushing failure when tested without the steel tube, Fig. 3.6. The compressive strength of concrete is almost the same as that found in a separate series of compression tests indicating that the presence of steel jacket does not adversely affect the behavior of concrete specimen. Fig. 3.7 shows the endochronic curve fit obtained for the steel fiber reinforced concrete. The constants for the biaxial and triaxial cases could not be determined due to the lack of experimental data in those load cases. Those constants were assumed to be same as those for plain concrete reported by Bazant and Shieh (1978). The constants obtained are as follows:

$a_o = 0.65$, $a_1 = 0.68/f'_c$,

$a_2 = 1175\,(\frac{f'_c}{4650})^{\frac{1}{2}}$; $a_3 = 324000/(f'_c)^4$;

$a_4 = 0.045$, $a_5 = 2160/(f'_c)^2$;

$a_6 = 0.15/(f'_c)^2$; $a_7 = 0.05$,

$a_8 = \frac{15}{f'^2_c}(\frac{f'_c}{3600})^{1.5}$ $a_9 = 0.0015$,

$a_{10} = 0.000125$, $a_{11} = 0.2/f'_c$,

$a_{12} = 0.8/f'_c$, $a_{13} = 2.2\times10^{-5}/f'_c$,

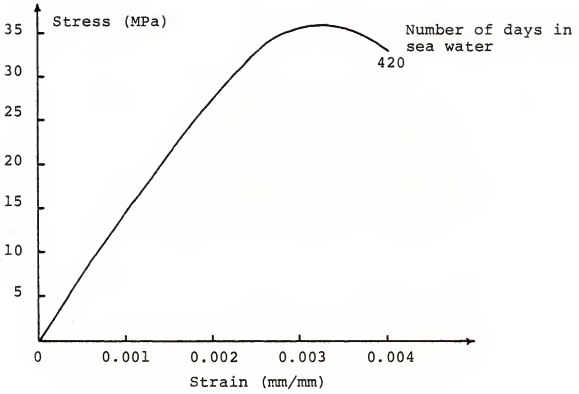

Fig. 3.3 Stress-Strain Behavior of Plain Concrete

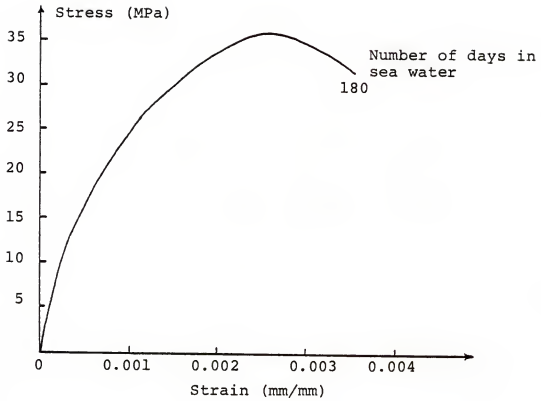

Fig. 3.4 Stress-Strain Behavior of Hooked-end Steel Fiber Reinforced Concrete

Fig. 3.5 Crack Pattern in the Failed Specimens Tested with Steel Tube

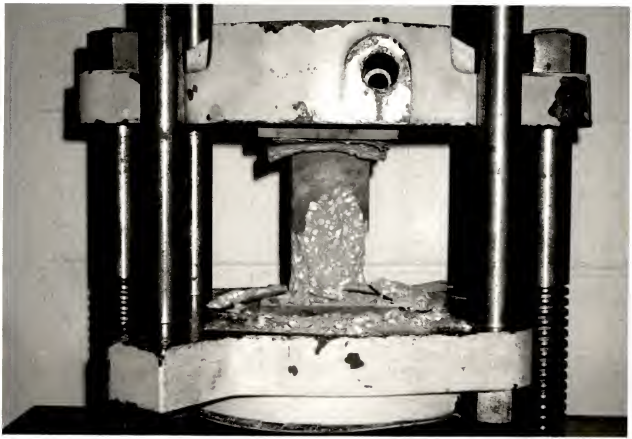

Fig. 3.6 Crack Pattern in the Failed Specimen Tested without Steel Tube

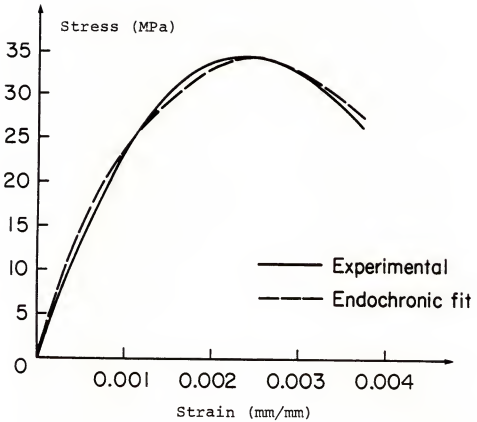

Fig. 3.7 Endochronic Curve Fit for Hooked-end Steel Fiber Reinforced Concrete

$a_{14} = 25.0$, $a_{15} = 1.095$,

$a_{16} = 1.216$, $a_{17} = 0.055$,

$a_{18} = 0.94$, $a_{19} = 6300/(f'_c)^2$,

$a_{20} = 14.0$, $a_{21} = 1000.0$,

$a_{22} = 0.04$, $a_{23} = 0.2\ f'_c$,

$b_1 = 9.1\ (\frac{f'_c}{7029})$, $b_2 = f'_c$,

$c_1 = 2.0/f'_c$, $c_2 = 0.003$,

$c_3 = 0.50$, $c_4 = 2.0$,

$c_5 = 250.0$, $c_6 = 0.002$,

$c_7 = 1.052 \times 10^{-6}$, $c_8 = 0.001$,

$\beta_1 = 30.0$, $\beta_2 = 3500.0$,

$\beta_3 = 0.08$, $\beta_4 = 0.23$,

$z_1 = 0.0015$, $z_2 = 0.0125$,

$\lambda_o = 0.007$, $\lambda'_o = 0.007$,

and

$$\nu = 0.182.$$

The initial slope formula used was that given by ACI,

$$E_o = 57{,}000\ \sqrt{f'_c} \qquad (3.11)$$

where

f'_c = compressive strength of concrete (psi).

Fig. 3.8 shows the predicted cyclic compressive stress-strain behavior under uniaxial loading. The curves were obtained by a strain control procedure using the constants determined above. The predicted closed hysteresis loops prove the superiority of the model compared to the earlier versions as indicated by Bazant and Shieh (1978).

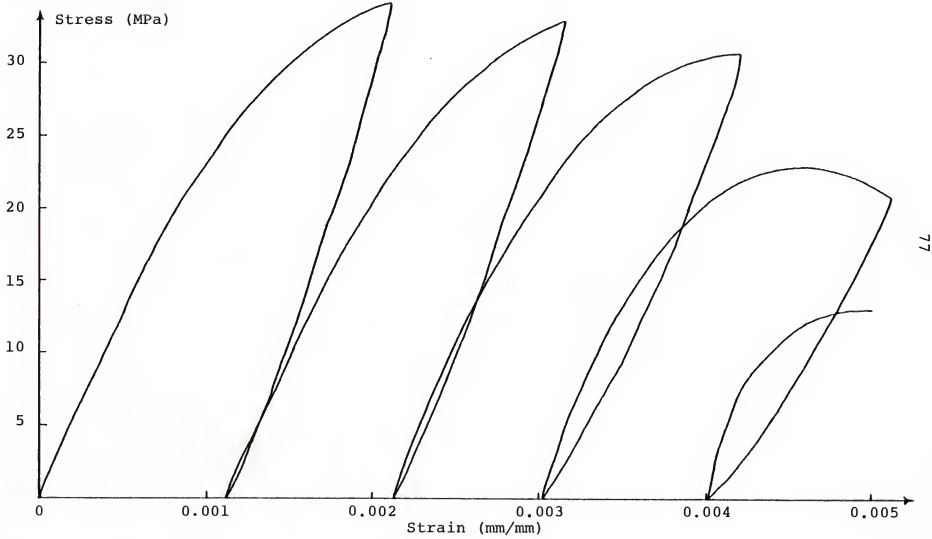

Fig. 3.8 Predicted Hysteresis Behavior Under Uniaxial Compression

CHAPTER IV
FLEXURAL BEHAVIOR OF FIBER REINFORCED CONCRETE BEAMS

4.1 Introduction

The load-deflection behavior of steel fiber reinforced concrete beams is predicted based on the endochronic theory for concrete discussed in the previous chapter and a probabilistic model for the fiber action. Analytical predictions are compared with the experimental data.

4.2 Material Models

4.2.1 Endochronic theory for concrete

The endochronic formulation described in Section 3.3 is used, with the constants for steel fiber reinforced concrete given in Section 3.6.

4.2.2 Model for fiber action

Fibers are assumed to participate only in the tensile region. Their effect in compression is accounted for by curve-fitting the stress-strain behavior under compressive loading. A crack is assumed to form normal to the principal stress when it exceeds the tensile strength of concrete. Experimental data on the fiber pull-out force and the crack opening displacement (COD) for steel fibers were reported by

Naaman and Shah (1976), and Matsuishi and Iwata (1982). Before the full interfacial bond strength, τ , is developed, the fiber force is linearly proportional to the crack opening and then it gradually decreases with a further increase in the crack opening. When the bond stress exceeds the limiting value τ , fiber force is found from the following expression proposed by Wecharatana and Shah (1983):

$$\sigma = \sigma_{max} \left(1 - \frac{\eta}{\eta_{max}} \right)^2 \qquad (4.1)$$

where

σ = fiber stress,

σ_{max} = fiber stress when the full interfacial bond strength is developed,

$= \tau \frac{\ell}{d}$

η = crack mouth displacement,

η_{max} = maximum pull-out displacement of fiber,

$= \ell/4$

and

ℓ,d = length and diameter of fiber respectively.

The total tensile resistance provided by the fibers is computed by considering the probabilistic number of fibers which intersect a unit cross-sectional area as reported by Matsuishi and Iwata (1982) and Naaman, Moavenzadeh, and McGarry (1970) in the following form:

$$N_s = \frac{2V_f}{\pi d^2} \qquad (4.2)$$

where

N_s = number of fibers intersecting a unit cross-sectional area,

and

V_f = volume content of fibers.

4.2.3 Model for reinforcing bars

The reinforcing bars are assumed to behave elasto-plastically until the initiation of strain hardening. The strain hardening portion is modeled by the following method as proposed by Burns and Siess (1962):

$$f_s = f_y\{\frac{112(\varepsilon_s-\varepsilon_{sh}) + 2}{60(\varepsilon_s-\varepsilon_{sh}) + 2} + \frac{\varepsilon_s-\varepsilon_{sh}}{\varepsilon_u-\varepsilon_{sh}}(\frac{f_u}{f_y} - 1.7)\} \qquad (4.3)$$

where

f_s = stress in the steel corresponding to a strain of ε_s,

f_y = yield stress of steel,

ε_{sh} = strain at which the hardening will commence,

and

ε_u = strain at ultimate stress of steel.

If the strain exceeds the yield value in one direction of loading, the stress-strain curve would no longer be elasto-plastic due to the Bauschinger effect; it will be a function of the residual strain for the load reversal. Upon load reversal, the following expression is used for stress between zero and yield

$$f_s = f_y[\,1 - \exp(\frac{-2.05\ \varepsilon_s}{\varepsilon'_{sh}}) + \frac{0.129\ \varepsilon_s}{\varepsilon'_{sh}}\,] \qquad (4.4)$$

where

ε'_{sh} = effective strain hardening strain

It is a function of the load history and the initial plastic strain ε_{ip}, defined as the difference in strain between two sequential points of zero stress immediately preceding a given load cycle expressed as follows:

$$\varepsilon'_{sh} = \frac{\varepsilon_{sh}}{1.38} \ln\frac{\varepsilon_{ip}}{\varepsilon_y} \tag{4.5}$$

When the stresses are greater than yield stress on the reversal, the virgin stress-strain curve is used by substituting ε'_{sh} for ε_{sh} in Eq. 4.3. A perfect bond is assumed between the reinforcing bars and concrete.

4.3 Load-deflection Relations of Beam

A layered beam element approach is used, which is similar to those used in earlier investigations, e.g. Park, Kent, and Sampson (1972). The internal moment for any given curvature increment is determined by satisfying the equilibrium of the cross section. Each section is divided into layers within which the strain is assumed to be constant. The moment developed at the center of the beam for any curvature increment is prorated to different sections along the length to determine the corresponding curvatures. The central deflection is found on the basis of the curvatures at different sections. The description in this section closely follows that of Bazant and Bhat (1972), except for the inclusion of fiber effects and the deflection calculations.

4.3.1 Incremental equilibrium equations

When the concrete is uncracked it is modeled as an isotropic material. The stress and strain are related as:

$$\{d\sigma + d\sigma''\} = [\,D\,]\ \{d\varepsilon\} \tag{4.6}$$

where

$d\sigma$, $d\sigma''$ = elastic and inelastic stress increments,

D = material property matrix,

and

$d\varepsilon$ = strain increment.

For uncracked concrete, D is written as follows:

$$[\,D\,] = \begin{bmatrix} D_{11} & D_{12} & D_{13} & 0 & 0 & 0 \\ & D_{22} & D_{23} & 0 & 0 & 0 \\ & & D_{33} & 0 & 0 & 0 \\ & & & D_{44} & 0 & 0 \\ & & & & D_{55} & 0 \\ & & & & & D_{66} \end{bmatrix} \tag{4.7}$$

where $D_{11} = D_{22} = D_{33} = K + \frac{4}{3} G$,

$D_{12} = D_{13} = D_{23} = K - \frac{2}{3} G$,

$D_{44} = D_{55} = D_{66} = 2G$,

G, K = shear and bulk moduli of concrete determined from the endochronic theory.

Inelastic stresses are determined from Eqs. 3.1a and 3.1b as follows:

$$d\sigma''_{ij} = 2G\, de^{p}_{ij} + 3K\, d\varepsilon^{p}\, \delta_{ij} \tag{4.8}$$

When the principal stress exceeds the tensile strength of concrete, cracks are assumed to form normal to

the maximum principal stress direction. After cracking, concrete is modeled as an orthotropic material, with zero stress across the crack. The concrete modulus matrix in the local coordinate system of cracks shown in Fig. 4.1 is given as follows:

$$[D'] = \begin{bmatrix} 0 & 0 & 0 & 0 & 0 & 0 \\ & D'_{22} & D'_{23} & 0 & 0 & 0 \\ & & D'_{33} & 0 & 0 & 0 \\ & & & \alpha D_{44} & 0 & 0 \\ & & & & \alpha D_{55} & 0 \\ & & & & & D_{66} \end{bmatrix} \qquad (4.9)$$

where

$$D'_{22} = D_{22} - \frac{D_{12}^2}{D_{11}},$$

$$D'_{23} = D_{23} - \frac{D_{13}D_{21}}{D_{11}},$$

$$D'_{33} = D_{33} - \frac{D_{31}^2}{D_{11}}$$

and

α = shear transfer factor.

[D'] matrix is obtained by a transformation of the matrix [D] to account for the loss of stiffness normal to the crack plane. Shear transfer factor is needed to account for the frictional force along the crack plane. A value of 0.5 is used for α, reported to be a reasonable value by Suidan and Schnobrich (1973). The cracked concrete modulus matrix [D'] is transformed back to the global coordinates by the

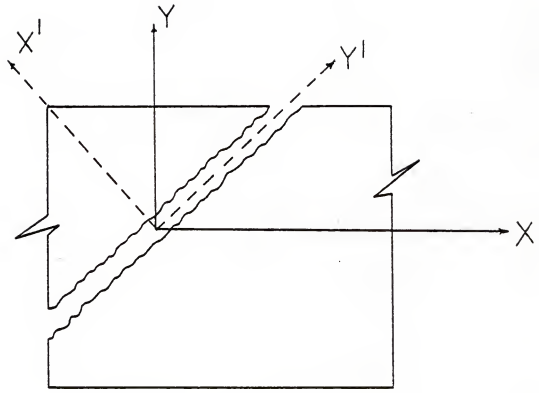

Fig. 4.1 Local Coordinate System for Crack

matrix [L] of the direction cosines of the principal stresses as follows:

$$[D''] = [L]^T [D'] [L] \qquad (4.10)$$

[D''] is used in Eq. 4.6 in place of [D] when a crack occurs.

Fig. 4.2 shows the coordinate system for the beam. The cross sections of the beam are assumed to remain plane after bending. The shear strains, ε_{xy}, ε_{yz}, and ε_{zx}, and the transverse normal strains, ε_{yy} and ε_{zz}, are taken into consideration in the analysis. They are assumed to be constant throughout each cross section. Both curvature and normal shear ε_{xz}, are assumed to contribute to deflections.

The longitudinal normal strain at any level of beam z_i can be written as follows:

$$d\varepsilon_{xx_i} = de - z_i\, dk \qquad (4.11)$$

where

$d\varepsilon_{xx_i}$ = incremental longitudinal strain at a distance z_i from the reference axis,

de = incremental longitudinal normal strain at the reference axis,

and

dk = incremental curvature of the beam.

The shear strains, ε_{xy} and ε_{yz}, and the corresponding shear stresses can be neglected for in-plane loading of the beam in xz-plane, Fig. 4.2. Then the cross-sectional equilibrium equations can be written in the following form:

$$dM = \sum_i z_i A_{x_i} d\sigma_{xx_i} + \sum_i z_i\, dF_{x_i}, \qquad (4.12)$$

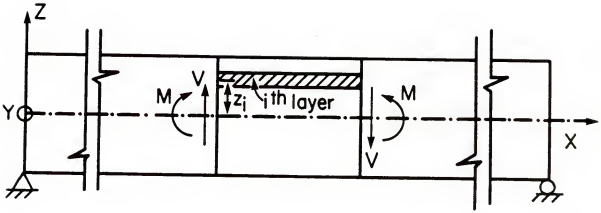

Fig. 4.2 Coordinate System for Beam
- Bazant and Bhat (1977)

$$dN_x = \sum_i A_{x_i}\, d\sigma_{xx_i} + \sum_i dF_{x_i} \tag{4.13}$$

$$dN_y = \sum_i A_{y_i}\, d\sigma_{yy_i} + \sum_i dF_{y_i} \tag{4.14}$$

$$dN_z = \sum_i A_{z_i}\, d\sigma_{zz_i} + \sum_i dF_{z_i} \tag{4.15}$$

and

$$dV = \sum_i A_{x_i}\, d\sigma_{xz_i} \tag{4.16}$$

The summation is carried out on all the layers. A_{x_i}, A_{y_i}, and A_{z_i} are the areas of the layers in the yz, xz, and xy planes respectively.

dF_{x_i} = longitudinal tensile force developed by the fibers in the case of a crack opening

$$= \eta\, N_s\, \frac{\pi}{4}\, d^2\, E_f\, d\varepsilon_{xx_i}$$

dF_{y_i} = tensile force developed by the fibers in the y-direction in the case of a crack opening

$$= \eta\, N_s\, \frac{\pi}{4}\, d^2\, E_f\, d\varepsilon_{yy_i}$$

and

dF_{z_i} = tensile force developed by the fibers in the z-direction in the case of a crack opening

$$= \eta\, N_s\, \frac{\pi}{4}\, d^2\, E_f\, d\varepsilon_{zz_i}$$

where

η = bond efficiency factor for the fibers, taken as 0.8,

and

E_f = Young's modulus of the fiber material.

By substituting the expressions for $d\sigma_{xx}$, $d\sigma_{yy}$, $d\sigma_{zz}$, and $d\sigma_{xz}$ in terms of de, dk, $d\varepsilon_{yy}$, $d\varepsilon_{zz}$, and $d\varepsilon_{xz}$ into the cross-sectional equilibrium equations, 4.12 - 4.16, five simultaneous force equilibrium equations are obtained, represented in a matrix form as follows:

$$\{df^C\} = [\ R^C\ ]\ \{d\varepsilon\} - \{df''\}\ , \qquad (4.17)$$

$\{df^C\}^T$ = internal force vector of concrete

$= \{dM,\ dN_x\ ,\ dN_y\ ,\ dN_z\ ,\ dV\}$

$\{d\varepsilon\} = \{de,\ dk,\ d\varepsilon_{yy}\ ,\ d\varepsilon_{zz}\ ,\ d\varepsilon_{xz}\}$

$\{df''\}$ = vector of inelastic forces,

and

$[\ R^C\ ]$ = stiffness matrix due to concrete alone.

The force equilibrium equations for the reinforcing steel can also be written as:

$$\{df^S\} = [\ R^S\ ]\ \{d\varepsilon\} \qquad (4.18)$$

The total forces in the cross section are obtained as a sum of the contributions of concrete and steel, Eqs. 4.17 and 4.18, which yields

$$\{df\} = [\ R\ ]\ \{d\varepsilon\} - \{df''\} \qquad (4.19)$$

where

$$[\ R\ ] = [\ R^C\ ] + [\ R^S\ ]$$

Solution techniques for Eqs. 4.19 have been discussed at length by Bazant and Bhat (1977).

4.3.2 Determination of deflections

The bending moment at the center of the beam is prorated to two other sections, and the corresponding curvatures are determined. Then the central deflection is found by the moment-area method. The load acting on the beam is found from the central moment. The computer program discussed by Bazant and Bhat (1977) has been modified to include the fiber

effects and to predict the central deflections from the curvatures.

4.4 Experimental Investigation

The experimental data used was that from the author's tests on fiber reinforced concrete beams exposed to circulating sea water and that reported by other investigators. The experimental results of Hughes and Fattuhi (1977a) were used to check the computer program.

As part of this investigation, steel fiber reinforced beams made of the same mix described in Section 3.4, exposed to circulating sea water were considered. Details of the beams, shown in Fig. 4.3, are dimensions of 102x102x 357 mm (4x4x12 in.), reinforced on both the compression and tension sides with steel bars of diameter 6.4 mm (#2 bars) and provided with stirrups of diameter 3.2 mm (#1 bars) at a spacing of 45 mm (1.8 in.). They were tested in 3-point loading over a span of 305 mm (12 in.) at a constant deflection rate of 1.25 mm (0.05 in.) per minute. The tests were carried out in a Tinius Olsen fixed head hydraulic testing machine of capacity 267 kN (60,000 lb.). The central deflection of the beam was measured as the machine head movement to an accuracy of 0.025 mm (0.001 in.) by a mechanical deflection gage as shown in Fig. 4.4. Three beams of each kind were tested and the average values reported. The tensile strength of the concrete was obtained by testing

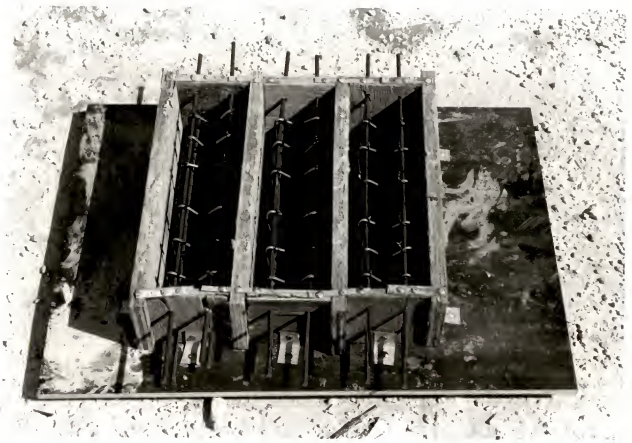

Fig. 4.3 Reinforcement Details for Test Beams

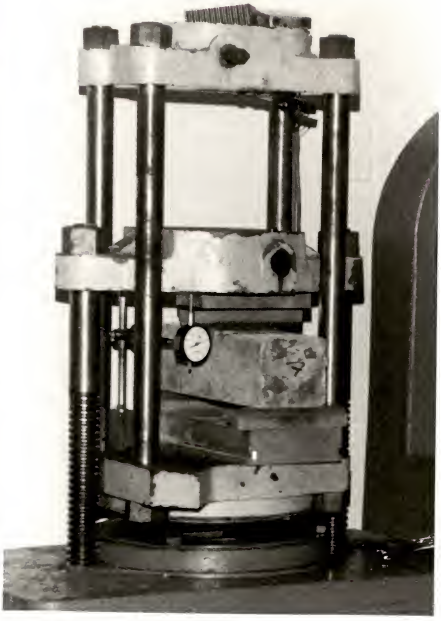

Fig. 4.4 Experimental Set-up for the Flexural Tests

cylindrical specimens of diameter 76.2 mm (3 in.) and length 152.4 mm (6 in.) under split cylinder tension, Fig. 4.5.

The experimental load-deflection curves reported by Hughes and Fattuhi (1977a) were obtained by testing beams of dimensions 102x102x508 mm (span = 406 mm) under third point loading. The specimens were reinforced with 1.5 precent by volume of Duoform (0.64x59 mm) and crimped (0.51x49 mm) steel fibers. Stress-strain curves for these two concretes, used to determine the endochronic constants, were obtained by testing cubes of 102 mm, Hughes and Fattuhi (1977c).

4.5 Results and Discussion

Figs. 4.6 and 4.7 show the experimental load-deflection (L-D) behavior of plain and hooked-end steel fiber reinforced concrete beams respectively. Ductility imparted due to steel fibers is evident from the larger area under L-D curve for steel fiber beams. Average pseudo-toughness index values for plain and steel fiber concrete beams, 4.5 and 7.0 respectively, very well reflect on the improvement due to fiber addition. The pseudo-toughness index is defined as the ratio of area under L-D curve to 80 percent of peak load on unloading branch and the area under L-D curve to first crack.

The comparison between the experimental and predicted behavior of crimped, Duoform, and hooked-end steel fiber concrete beams is shown in Figs. 4.8, 4.9, and 4.10 respectively. The model over-predicts for crimped fibers,

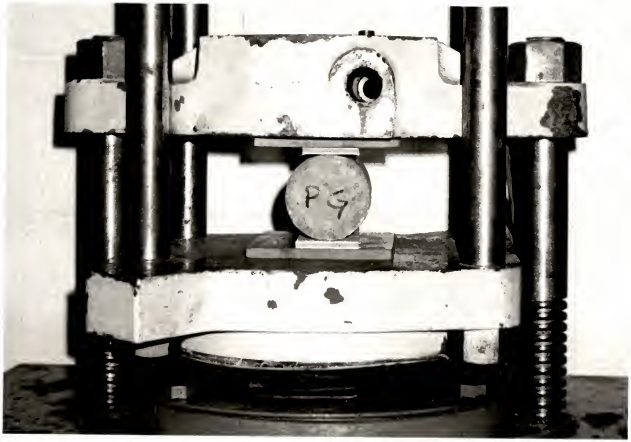

Fig. 4.5 Experimental Set-up for the Split Cylinder Tension Tests

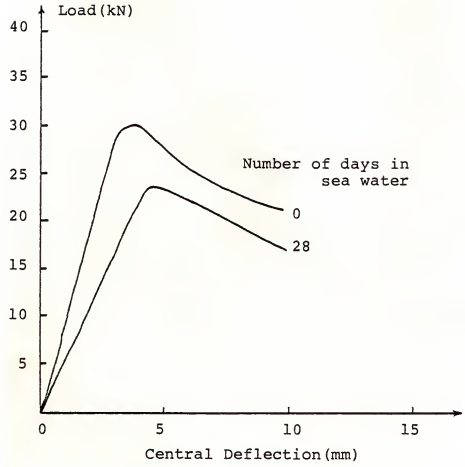

Fig. 4.6 Flexural Behavior of Plain Concrete Beams

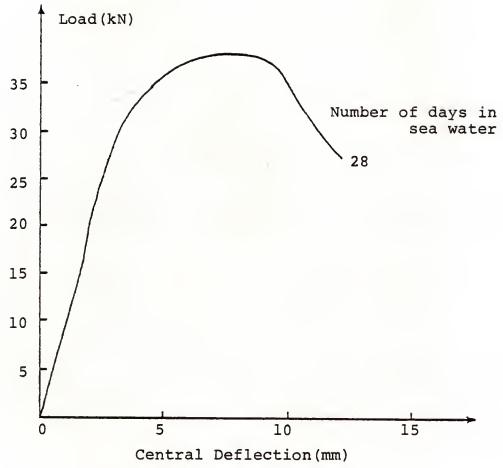

Fig. 4.7 Flexural Behavior of Hooked-end Steel Fiber Concrete Beams

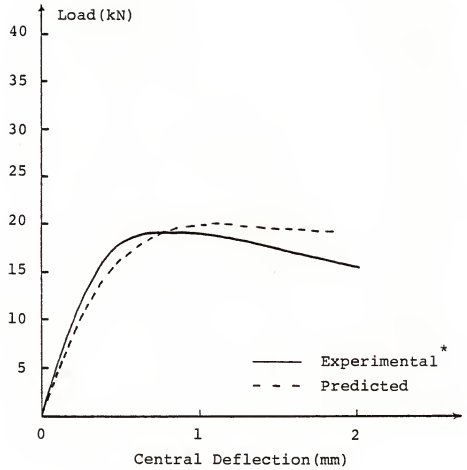

Fig. 4.8 Predicted and Experimental Flexural Behavior of Crimped Steel Fiber Concrete Beams

*From Hughes and Fattuhi (1977a)

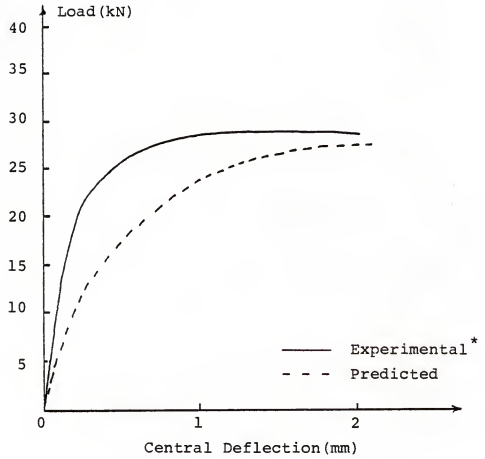

Fig. 4.9 Predicted and Experimental Flexural Behavior of Duoform Steel Fiber Concrete Beams

*From Hughes and Fattuhi (1977a)

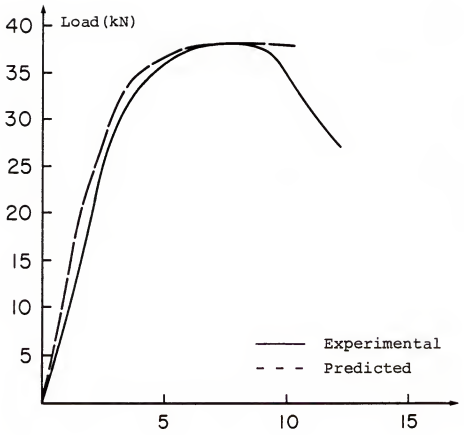

Fig. 4.10 Predicted and Experimental Flexural Behavior of Hooked-end Steel Fiber Concrete Beams

under-predicts for Duoform fibers, and gives almost exact values for hooked-end steel fibers. This seems to be due to the inadequate modeling of fiber action. Duoform fibers are a special type with high bond strength in contradistinction to crimped fibers in which the stress concentrations cause matrix cracking and disbonding of fibers. The bond properties assumed in the model are more relevant to the hooked-end steel fibers as indicated by the good agreement in Fig. 4.10. In the ideal case, fiber pull out load- slip distance curves for each kind should be incorporated in the model which would lead to improved predictions.

CHAPTER V
ENDOCHRONIC FINITE ELEMENT ANALYSIS OF A FROZEN SOIL FOUNDATION

5.1 Introduction

Most of the offshore drilling concepts in Frontier areas are of the gravity type, e.g., artificial islands and concrete gravity platforms in relatively shallow water and subject to large ice and wave forces. Artificial islands have been reported to be more economical in terms of construction and maintenance costs in water depths of less than 20 m. (66 ft.), Robertson (1983). In the foundation design of these structures, which are close to the shore, advantage can be taken of the high strength frozen-soil layers. If the thermal structure is not disturbed these layers provide a firm base for foundation over a long duration of time.

A frozen-soil is a thermal condition of the ground in which the soil is perennially frozen. It occurs in the areas where the soil temperatures of $0^{\circ}C$ ($32^{\circ}F$) and below persist over two consecutive winters and the intervening summer. It consists of solid mineral particles, ice, liquid (unfrozen) water, and gaseous inclusions. The properties of it are highly dependent on the volume contents of various

constituents and temperature. Blouin et al. (1979) reported the occurrence of subsea frozen-soil layers in the Prudhoe Bay, Alaska.

5.2 Stress-Strain Relations

Experimental data on frozen soils obtained by many investigators suggest that its behavior is highly dependent on the test temperature and rate of loading, Ladanyi (1981), Parameswaran (1980), and Parameswaran and Jones (1981). Since ice is the main internal bonding agent, even a slight change in the temperature could change the degree of cementation, affecting the properties in an adverse manner. Parameswaran (1980), in his experiments on frozen-soil samples, found that the specimens deform elastically in the early stages of deformation when strain is less than one percent. As the strain rate increases, the specimens show an upper yield point, and fail essentially in a brittle manner. The failure stress increased with increasing rates of strain and decreasing temperatures.

To model the strain rate effects and temperature, stress-strain relations for concrete Eqs. 3.1a and 3.1b are modified in a simplistic manner as follows:

$$de_{ij} = de^{e}_{ij} + de^{p}_{ij} = \frac{ds_{ij}}{2G} + \frac{s_{ij}}{2G}\, dZ, \qquad (5.1a)$$

$$d\varepsilon = d\varepsilon^{e} + d\varepsilon^{p} = \left(1 + t_1 e^{t_2 \theta} \right) \frac{d\sigma}{3K} + d\lambda + \frac{\sigma}{3K}\, dZ' + d\lambda' + \frac{\sigma}{3K} \frac{dt}{\tau_1} \qquad (5.1b)$$

The thermal effect is incorporated into the incremental volumetric strain. This enables higher strain increments with higher temperatures for the same volumetric stress increment. The thermal strains in frozen soil are regarded as inelastic in view of their irreversible nature. The intrinsic times dZ and dZ' are redefined as follows to include the time effects:

$$(dz)^2 = \left(\frac{d\tau}{z_1}\right)^2 + \left(\frac{dt}{\tau_1}\right)^2, \qquad (5.2a)$$

and

$$(dz')^2 = \left(\frac{d\tau'}{z_2}\right)^2 + \left(\frac{dt}{\tau_1}\right)^2, \qquad (5.2b)$$

where

dt = time increment $= \frac{d\varepsilon}{\dot{\varepsilon}}$

$\dot{\varepsilon}$ = strain rate,

τ_1 = time hardening function for creep,

$= \tau_a + \tau_b(t - t_o)$

t_1 , t_2 = constants to be determined,

θ = temperature in ^oC,

and

τ_a, τ_b = constants to be determined.

This formulation is only valid for negative temperatures. The time hardening function for creep, τ_1 , makes the rate of creep decrease with time, which is commonly observed in the experiments. This method is the same as that applied to concrete by Bazant and Bhat (1976).

5.3 Experimental Data

The experimental data used in this investigation is that obtained by Parameswaran (1980), and Parameswaran and Jones (1981) from tests on cylindrical specimens of diameter 50.8 mm (2 in.) and length 140 mm (5.5 in.) with 20 percent moisture content, and a bulk density of $20 kN/m^3$ ($127 lb/ft^3$). The tests were carried out at different temperatures and strain rates. The uniaxial stress-strain curve was obtained by testing the specimens at a temperature of -6^oC (21.2^oF) at a strain rate of 3.98×10^{-5} per second. The triaxial curve was obtained at a temperature of -10^oC (14^oF) at a strain rate of 7.7×10^{-5} per second and a hydrostatic confining pressure of 0.1 MPa (15 psi.)

5.4 Determination of Endochronic Constants

The endochronic constants are determined as described in Section 3.5. Figs. 5.1 and 5.2 show the curve fits obtained for the uniaxial and triaxial stress-strain curves. The lack of a good fit for the triaxial curve shows the limitation of the model. The curve fit could be improved by constructing some other functions to take into account the melting of intergranular ice at high pressures; this requires a stronger dependency on the temperature and hydrostatic pressure. Various constants obtained are as follows:

$$a_o = 0.52, \qquad a_1 = 0.41/f'_c,$$

$$a_2 = 750\left(\frac{f'_c}{4650}\right)^{\frac{1}{2}}, \qquad a_3 = 252{,}000/(f'_c)^4,$$

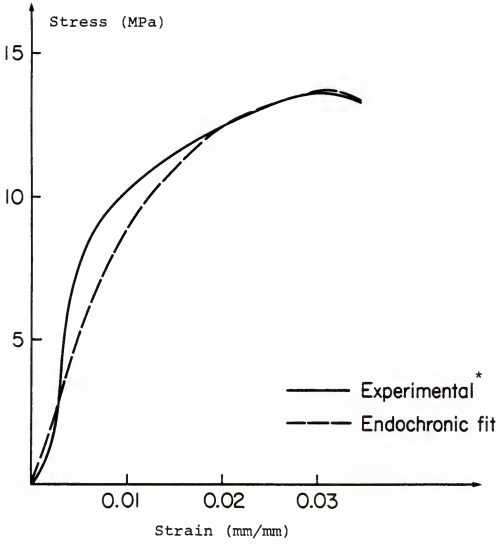

Fig. 5.1 Uniaxial Stress-Strain Curve Fit for Frozen Soil

*From Parameswaran (1980)

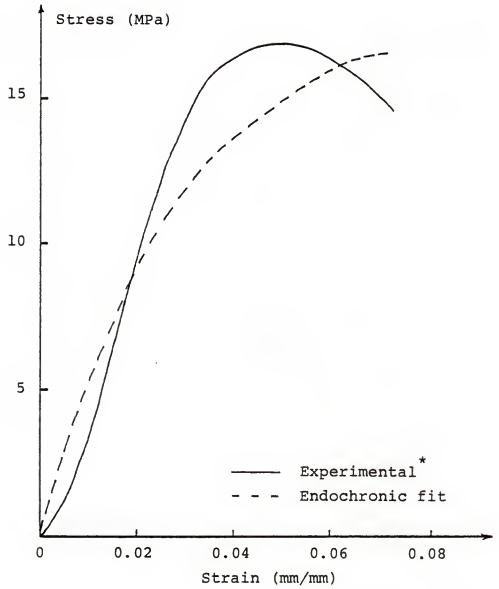

Fig. 5.2 Triaxial Stress-Strain Curve Fit for Frozen Soil

*From Parameswaran and Jones (1981)

$a_4 = 3.0,$ $a_5 = 28{,}800/(f'_c)^2,$

$a_6 = 0.001/(f'_c)^2,$ $a_7 = 0.763,$

$a_8 = \frac{2.5}{f'^2_c}\left(\frac{f'_c}{3600}\right)^{1.5}$ $a_9 = 0.00145,$

$a_{10} = 0.000158,$ $a_{11} = 7.0/f'_c,$

$a_{12} = 3.5/f'_c,$ $a_{13} = 0.01\times10^{-5}/f'_c,$

$a_{14} = 5.0,$ $a_{15} = 0.095,$

$a_{16} = 1.216,$ $a_{17} = 1.50,$

$a_{18} = 0.50,$ $a_{19} = 6300/(f'_c)^2,$

$a_{20} = 14.0,$ $a_{21} = 1000.0,$

$a_{22} = 0.01,$ $a_{23} = 0.4\ f'_c,$

$b_1 = 5.5\left(\frac{f'_c}{7020}\right),$ $b_2 = 4.0\ f'_c,$

$c_1 = 7.5/f'_c,$ $c_2 = 0.009,$

$c_3 = 0.15,$ $c_4 = 0.50,$

$c_5 = 21.0,$ $c_6 = 0.002,$

$c_7 = 2.5\times10^{-6},$ $c_8 = 0.01,$

$\beta_1 = 50.0,$ $\beta_2 = 2{,}500.0,$

$\beta_3 = 0.04,$ $\beta_4 = 0.15,$

$Z_1 = 0.003,$ $Z_2 = 0.023,$

$\lambda_o = 0.006,$ $\lambda'_o = 0.006,$

$\tau_a = 0.50,$ $\tau_b = 0.85,$

$t_1 = 1.25,$ and $t_2 = 0.15.$

The initial slope used is that of the uniaxial curve, E = 338,285 psi. and the Poisson ratio = 0.30.

5.5 Finite Element Analysis of Structural Response

A finite element computer program has been developed based on the endochronic stress-strain behavior described in Section 5.2. It can account for the time-dependent creep and thermal effects. Constant strain axisymmetric elements are used, but the two-dimensional problems can also be analyzed by deleting the ε_θ term from the element equations. For any given load increment, the nodal displacements and the element stresses are found by an iterative procedure. For any constant set of loads, the creep response can be found by incrementing the time 'dt' in Eqs. 5.2a and 5.2b. The computer program developed in this section closely follows that of Bazant and Shieh (1978). The accuracy of the program is checked with the results presented for a strip footing by Haldar, Reddy, and Arockiasamy (1982).

The foundation response to the static weight of a typical Arctic offshore island is obtained by the computer program discussed above. Details of the island as reported by Róbertson (1983), are a diameter of 107 m. (350 ft), finished elevation of 4 m. (13 ft) above the mean sea level, water depth of 3.35 m. (11 ft), and approximately 120,035 m^3 (157,000 yd^3) of gravel. Fig. 5.3 shows the finite element discretization of the foundation. All the nodes on the two sides and the bottom are assumed to be supported on rollers. The soil is assumed to have a constant temperature over the

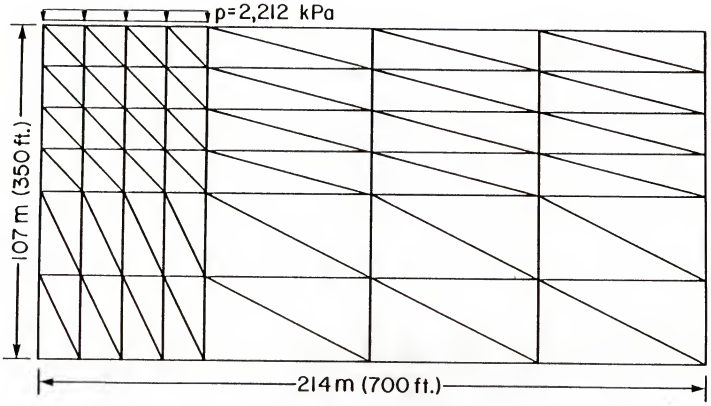

Fig. 5.3 Finite Element Discretization of the Foundation

entire depth of the foundation. If the temperature profile is known, exact temperatures can be specified for each element separately.

5.6 Results and Discussion

Fig. 5.4 shows the deflection profile at $-6^{o}C$ ($21.2^{o}F$) temperature at various times. Figs. 5.5 and 5.6 show the deflection profiles at different temperatures and times.

As expected, the deflections are larger at higher temperatures. The strength and the initial slope of the stress-strain curve of the frozen soil decrease with an increase in the temperature. This is clearly verified by the higher initial and creep-induced deflections for higher temperatures. With a decrease in the temperature, the properties of the frozen soil reach steady state values, which will not change considerably even with further temperature reductions. This is well reflected by the proximity of the deflections at $-6^{o}C$ and $-15^{o}C$ temperatures.

The extension of the endochronic constitutive modeling to include creep and thermal effects seems reasonable, but needs to be studied in greater detail with actual field data and compared with other analytical approaches.

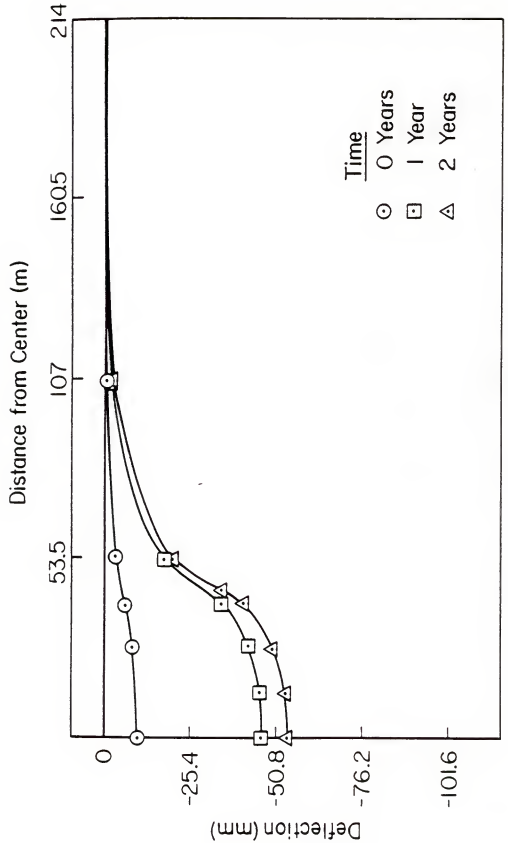

Fig. 5.4 Deflection Profiles at Different Times at Soil Temperature = $-6^{o}C$

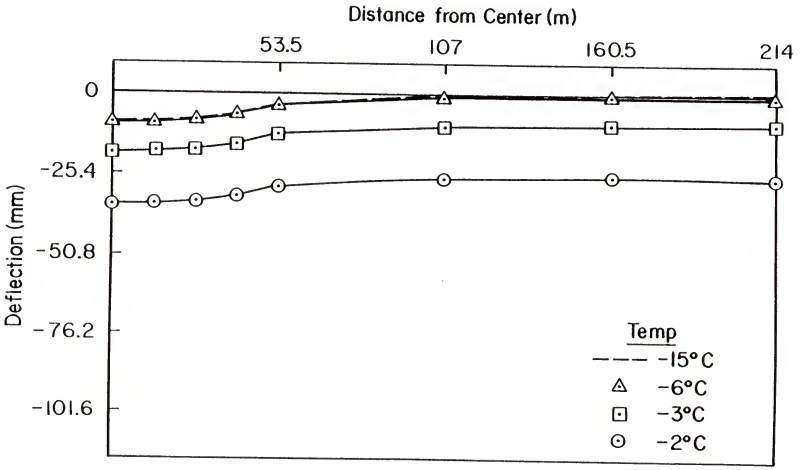

Fig. 5.5 Deflection Profiles at Time = 0 for Different Soil Temperatures

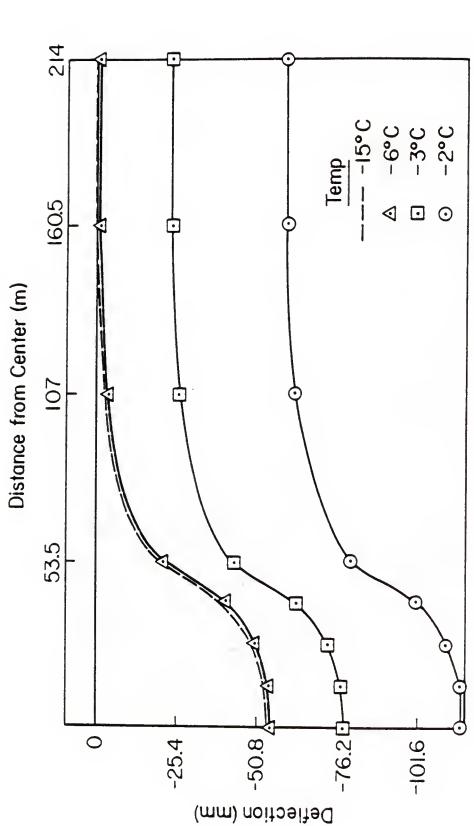

Fig. 5.6 Deflection Profiles at Time = 2 years for Different Soil Temperatures

CHAPTER VI
SUMMARY & CONCLUSIONS

This work has been an investigation on the application of endochronic theory to the analysis of marine exposed fiber concrete structural components in conjunction with a probabilistic method to account for the fiber effects and an extension of the endochronic formulation by including the thermal and creep effects. This chapter summarizes the findings of this investigation and scope for further research in this area.

6.1 Summary

Initially, a brief review of the present state of the art is made on various topics pertaining to this investigation, i.e., marine concrete behavior, fiber reinforced concrete, constitutive models, and concrete structural analysis techniques. It was observed that, although considerable work has been carried out on developing models for the fiber concretes in cyclic loading and the methods to predict the additional load carrying capacity due to fibers, not much has been done in applying these in incremental structural analysis programmes. Most of these theories tend to be

based on the particular experimental data of the investigator and may not be realistic for other fiber types.

The endochronic formulation for concrete seems to be the most comprehensive of all the constitutive theories capable of modeling the experimentally observed nonlinearities of concrete, i.e., strain hardening, softening, dilatancy due to internal microcracking, and hydrostatic pressure sensitivity. The only variable which needs to be specified to describe the behavior of any normal weight plain concrete is its compressive strength. It was reported that the predicted concrete stress-strain behavior based on its compressive strength compares well with the experimental data and with that obtained by the expression of Popovics (1973). The formulation for concrete has excellently predicted the hysteretic flexural behavior of beams, Bazant and Bhat (1977). These two aspects of the theory prove its predictive capabilities in contrast to the usually misconstrued belief that it is a just another curve-fitting model.

The recently developed endochronic models which overcome the deficiencies of the earlier formulations are evaluated along with some of their applications. Bazant (1978) introduced the concept of jump-kinematic hardening into the endochronic theory to achieve closed hysteresis loops. Valanis (1980) achieved the same by redefining the intrinsic time in terms of plastic strains instead of the total strain. Internal constraints in these two formulations

require an additional computational effort, but still preserve the continuous modeling feature of the theory.

Complete stress-strain curves were obtained by testing the concrete specimens in parallel with a coaxial special alloy steel tube. This technique was found to produce a stable descending portion of the curve irrespective of the machine characteristics. By comparing the compressive strengths with those obtained in separate compression tests without steel tube, it was concluded that the concrete behavior is unaffected by the presence of steel tube. Similar conclusion was made by Wang, Shah, and Naaman (1978a) by comparing the ascending portion of many curves obtained with and without steel tube. Endochronic material constants were determined by curve-fitting the experimental data using an optimization process. The cyclic behavior of steel fiber concrete under uniaxial compression was predicted based on the constants determined from a data without cycling. Although, it could not be compared with any experimental curve due to nonavailability, the predicted cyclic behavior seems to be realistic.

The flexural behavior of steel fiber reinforced concrete was predicted based on the endochronic formulation for concrete together with a probabilistic model for the tensile contribution of fibers. The fiber model is based on the experimental data reported by various investigators on straight and hooked-end steel fiber concretes. The major factors involved are the probabilistic number of fibers intersecting a unit cross-sectional area, limiting stress at

which fiber debonding occurs, and the frictional shear stress after debonding. The present model is not valid for the cyclic loading cases since the tensile zone fiber behavior in unloading and reloading is not considered. The analytical behavior was compared with the experimental data for three different fiber kinds, hooked-end, crimped, and Duoform. As explained in Section 4.5, the model is quite accurate for hooked-end fibers, and for the others it differs by as much as 10 to 15 percent. This is due to the reason that the experimental data on those two fiber types are not incorporated into the model.

The endochronic theory presents a viable method for incorporating various features of material behavior into the constitutive equations. In Chapter 5, a simple method was proposed to include the thermal and creep behavior of materials like ice and frozen soil. The response of a typical Arctic island foundation consisting of frozen soil was analyzed by a finite element analysis program developed with the above constitutive law. Endochronic constants for the frozen soil were determined by curve-fitting uniaxial and triaxial stress-strain curves at different temperatures and strain rates. The results of this program have been found to compare favorably with those of ADINA (Automatic Dynamic Incremental Nonlinear Analysis) as shown by Gopal and Reddy (1985).

Appendix-A outlines the various numerical schemes used in the present investigation.

6.2 Suggestions for Further Studies

The following suggestions are made for future research efforts in this area:

1) A model should be developed for random fiber concretes after cracking under cyclic loading by adapting similar models for continuous fibers. This kind of a model is needed to study the behavior of fiber reinforced concrete structural elements subjected to dynamic loading.
2) It is desirable to simplify the present endochronic formulation for concrete to enable easy determination of the constants for new sets of data.
3) In view of its capabilities, endochronic theory provides a vast scope for developing accurate fracture analysis of fiber concretes. Most of the previous studies have been based on linear elastic methods which are not realistic for concrete due to its nonlinearities. Ductility due to fibers and the tensile softening in the matrix process zone near the crack tip can be easily accounted for by endochronic formulations.
4) Another interesting area of research is in the probabilistic characterization of the endochronic parameters by fitting largely scattered data from different sources. Then the statistical mean response of the structure and the associated reliability coefficients can be determined. Since each set of constants represents a particular type of behavior, the probabilistic endochronic approach would provide a good basis for this kind of analysis.

6.3 Conclusions

It is relevant to conclude this investigation with a philosophical remark that no single constitutive model can be expected to be valid under all possible circumstances. The fact that it may not be valid for some situations should not obscure its superiority and usefulness in other cases.

APPENDIX A
NUMERICAL IMPLEMENTATION TECHNIQUES

A.1 Stress-Strain Model

Stress-strain curves are generated by the endochronic formulation described in Section 3.3. The curve is generated by a strain control procedure in which the stresses corresponding to a given strain increment are found. Eqs. 3.1a and 3.1b can be written in an expanded form as follows:

$$\begin{bmatrix} \Delta\sigma_{11}+\Delta\sigma''_{11} \\ \Delta\sigma_{22}+\Delta\sigma''_{22} \\ \Delta\sigma_{33}+\Delta\sigma''_{33} \\ \Delta\sigma_{12}+\Delta\sigma''_{12} \\ \Delta\sigma_{23}+\Delta\sigma''_{23} \\ \Delta\upsilon_{31}+\Delta\sigma''_{31} \end{bmatrix} = \begin{bmatrix} D_1 & D_2 & D_2 & 0 & 0 & 0 \\ D_2 & D_1 & D_2 & 0 & 0 & 0 \\ D_2 & D_2 & D_1 & 0 & 0 & 0 \\ 0 & 0 & 0 & D_3 & 0 & 0 \\ 0 & 0 & 0 & 0 & D_3 & 0 \\ 0 & 0 & 0 & 0 & 0 & D_3 \end{bmatrix} \begin{bmatrix} \Delta\varepsilon_{11} \\ \Delta\varepsilon_{22} \\ \Delta\varepsilon_{33} \\ \Delta\varepsilon_{12} \\ \Delta\varepsilon_{23} \\ \Delta\varepsilon_{31} \end{bmatrix} \qquad (A.1)$$

in which

$$D_1 = K + \frac{4}{3} G,$$

$$D_2 = K - \frac{2}{3} G,$$

$$D_3 = 2 G,$$

$$\Delta\sigma''_{ij} = \text{inelastic stress increment}$$

$$= s_{ij}\, dZ + (3\, K\, d\lambda + 3\, K\, d\lambda' + \sigma\, dZ')\delta_{ij} \qquad (A.2)$$

$\Delta\sigma_{ij}$ = elastic stress increments,

$\Delta\varepsilon_{ij}$ = prescribed strain increments,

and

σ = volumetric stress.

Eq. A.1 is re-cast to have known quantities on the right hand side and unknown quantities on the left. For example, for a uniaxial case, all stresses except σ_{11} are zero and Eq. A.1 is rewritten in the following form:

$$\begin{bmatrix} 1 & -D_2 & -D_2 & 0 & 0 & 0 \\ 0 & -D_1 & -D_2 & 0 & 0 & 0 \\ 0 & -D_2 & -D_1 & 0 & 0 & 0 \\ 0 & 0 & 0 & -D_3 & 0 & 0 \\ 0 & 0 & 0 & 0 & -D_3 & 0 \\ 0 & 0 & 0 & 0 & 0 & -D_3 \end{bmatrix} \begin{bmatrix} \Delta\sigma_{11} \\ \Delta\varepsilon_{22} \\ \Delta\varepsilon_{33} \\ \Delta\varepsilon_{12} \\ \Delta\varepsilon_{23} \\ \Delta\varepsilon_{31} \end{bmatrix} = \begin{bmatrix} D_1\Delta\varepsilon_{11}-\Delta\sigma''_{11} \\ D_2\Delta\varepsilon_{11}-\Delta\sigma''_{22} \\ D_2\Delta\varepsilon_{11}-\Delta\sigma''_{33} \\ -\Delta\sigma''_{12} \\ -\Delta\sigma''_{23} \\ -\Delta\sigma''_{31} \end{bmatrix} \quad \text{(A.3)}$$

For other loading cases like biaxial or triaxial, Eq. A.1 can be rewritten in a similar fashion.

For any given strain increment in the r-th step, Eq. A.3 is solved iteratively. Based on the values of (r-1)th step, dZ, dZ', dλ, dλ', and D's are determined from Eqs. 3.2, 3.3, 3.4, 3.5 and 3.10 respectively. Then the inelastic stress increments $\Delta\sigma''_{ij}$ are determined from Eqs. A.2 and the elastic increments from Eqs. A.3. The iteration is continued until the stresses in two succeeding steps converge to within 1.0 percent.

A.2 Determination of Endochronic Constants

Endochronic constants are determined by an optimization process using an IMSL (international Mathematical and Statistical Library) subroutine, "ZXSSQ", based on the finite difference Levenberg-Marquardt algorithm. The stress-strain program is arranged as a subroutine, "FUNC", which computes the deviations of the response curves from the specified experimental data. This subroutine is called by the optimization subroutine, "ZXSSQ", which varies the endochronic constants to arrive at an optimal curve-fit. The flow chart in Fig. A.1 shows the sequence of operations involved.

A.3 Flexural Behavior of Beams

At each step the curvature at the center of the beam is incremented by 'dK' and the corresponding moment increment 'dM' is determined. This moment is prorated to other sections along the length and the corresponding curvatures are determined. Based on the curvatures at various sections along the length of the beam, central deflections are determined from the area-moment theorem. The procedure used is the same as that discussed in the next Section, A.4

A.4 Axisymmetric Finite Element Analysis

Plane strain axisymmetric elements, shown in Fig. A.2 are used in the analysis. The displacement field for the element is written as follows:

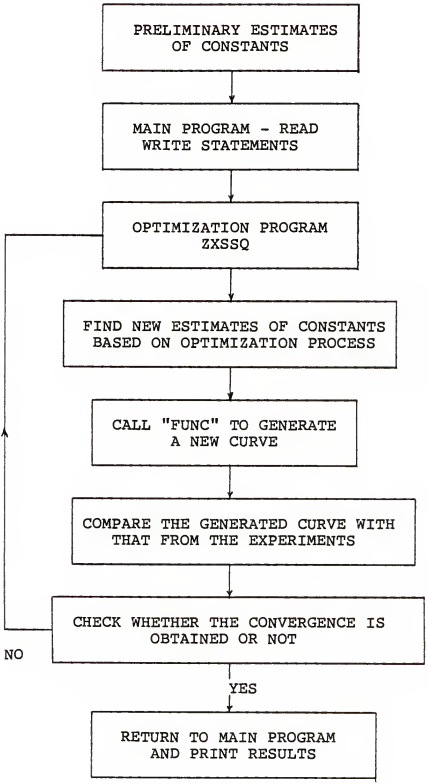

Fig. A.1 Flow Chart

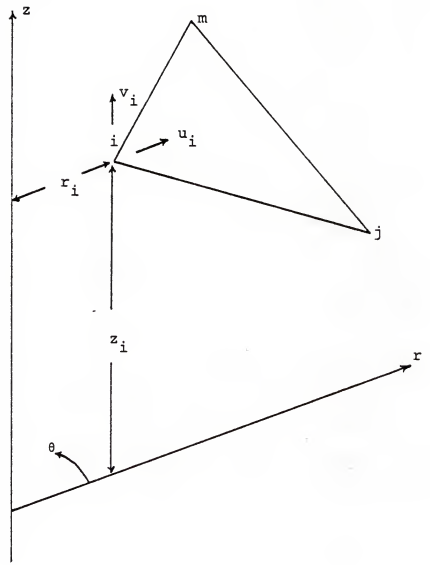

Fig. A.2 Axisymmetric Element

$$\underline{u} = \begin{bmatrix} u \\ v \end{bmatrix} = [\,N\,]\ \{a^e\} \qquad (A.4)$$

where

$[\,N\,]$ = shape function matrix, the elements of which are given as,

$$N_i = \frac{a_i + b_i r + c_i z}{2\Delta}$$

$$a_i = r_j z_m - r_m z_j$$

$$b_i = z_j - z_m$$

$$c_i = r_m - r_j$$

and

$\{a^e\}$ = element nodal displacements.

The strain vector is obtained as,

$$\underline{\varepsilon} = \begin{bmatrix} \varepsilon_z \\ \varepsilon_r \\ \varepsilon_\theta \\ \varepsilon_{rz} \end{bmatrix} = \begin{bmatrix} \frac{\partial v}{\partial z} \\ \frac{\partial u}{\partial r} \\ \frac{u}{r} \\ \frac{\partial u}{\partial z} + \frac{\partial v}{\partial r} \end{bmatrix} = [\,L\,]\ \{u\}$$

$$= [\,L\,]\,[\,N\,]\ \{a\} = [\,B\,]\ \{a\} \qquad (A.5)$$

The stress and strain are constitutively related as

$$\{d\sigma + d\sigma''\} = [\,D\,]\ \{d\varepsilon\} \qquad (A.6)$$

The stiffness matrix for the elements is written as follows:

$$K^e_{ij} = 2\pi \int [\,B\,]^T [\,D\,]\,[\,B\,]\, r\, dr\, dz \qquad (A.7)$$

The integral in Eq. A.7 is evaluated at the centroid of the elements,

$$\bar{r} = (r_i + r_j + r_m)/3 \qquad (A.8)$$

$$\bar{z} = (z_i + z_j + z_m)/3 \qquad (A.9)$$

which gives

$$K^e_{ij} = 2 \pi B_i^T D B_j \bar{r} \Delta \qquad (A.10)$$

where Δ is the area of the element.

The nodal forces due to a distributed load R, are written as follows:

$$\{f_i\} = 2 \pi r R \qquad (A.11)$$

The analysis steps for each load increment are as follows:

1) For each load increment dP, the nodal displacements are found from

$$[K] \{du\} = \{dP\} \qquad (A.12)$$

Then the element strain and stress increments are found as follows:

$$\{d\varepsilon\} = [L] \{du\} \qquad (A.13)$$

and

$$\{d\sigma\} = [D] \{d\varepsilon\} \qquad (A.14)$$

2) The principal strains at the center of each element are checked with the crushing strain of the material(input). If crushing occurs, then the stress vector, $\sigma_{i-1} + \Delta\sigma_i$ for the element is converted to nodal forces as

$$P_2^e = \int B^T (\sigma_{i-1} + \Delta\sigma_i) \, d(vol) \qquad (A.15)$$

This force system is redistributed back into the rest of the structure by step 4. The element stiffness and the updated stress vector are then set to zero.

3) If the principal stress is smaller than the tensile strength of the material, σ_t , and the element has not cracked before, step 4 is executed. If, however, the greatest principal stress is greater than σ_t , cracking is assumed to take place during the current iteration. For the case of no previous cracking the stress vector is evaluated as

$$\sigma_i = [\ D^e\ ]\ \{\varepsilon_{i-1} + d\varepsilon\} \tag{A.16}$$

If the element has cracked previously, then

$$d\sigma_i = [\ D''\ ]\ \{d\varepsilon_i\} \tag{A.17}$$

and

$$\sigma_i = \sigma_{i-1} + d\sigma_i \tag{A.18}$$

The [D"] matrix is formed from [D] in the same manner as shown in Eq. 4.10. The stress level that can exist in the element after cracking is computed and the residual stress vector is computed. The residual stress vector is converted to nodal forces and redistributed in the structure in step 4 as

$$P_2^e = \int [\ B\ ]^T \{\ \sigma_i - \sigma_{i-1} + d\sigma_i\}\ d(vol) \tag{A.19}$$

4) The equivalent nodal force vector for the entire structure is evaluated as

$$P = \sum_e \{P_1^e + P_2^e\} \tag{A.20}$$

If all the elements of P are less than or equal to Δ , the next load increment is applied to the structure and steps 1-4 are repeated. If any of the components of P are greater than Δ , the load P is applied to the structure and the element stresses and strains, and the nodal displacements are computed. This is repeated until all the components of P are insignificant.

All the above numerical schemes have been implemented on VAX VMS-11/780 computer systems at the University of Florida and Florida Atlantic University.

BIBLIOGRAPHY

American Concrete Institute Committee 544, "State of the Art Report on Fiber Reinforced Concrete," American Concrete Institute Journal, Vol. 70, No. 2, 1973, pp. 729-744.

American Concrete Institute Committee 544, "Measurement of Properties of Fiber Reinforced Concrete," American Concrete Institute Journal, Vol. 75, No. 7, 1978, pp. 283-289.

Ansal, A.M., Krizek, R.J., and Bazant, Z.P., "Seismic Analysis of an Earth Dam Based on Endochronic Theory," Proceedings of the International Conference on Numerical Models in Geomechanics, Eds. Dungar, R., Pande, G.N., and Studer, J.A., Rotterdam, The Netherlands, 1982, pp. 559-576.

Aveston, J., Cooper, G.A., and Kelly, A., "Single and Multiple Fracture," Proceedings of the Conference on the Properties of Fiber Composites, National Physical Laboratory, London, 1971, pp. 15-24.

Barab, S., and Hanson, D., "Investigation of Fiber Reinforced Breakwater Armor Units," Proceedings of the International Symposium on Fiber Reinforced Concrete, American Concrete Institute, Ottawa, Canada, 1973, pp. 415-434.

Bazant, Z.P., "Theory of Creep and Shrinkage in Concrete Structures," A Precis of Recent Developements, Mechanics Today, Ed. Nemat-Nasser, S., Pergamon Press, New York, N.Y., Vol. 2, 1975, pp. 1-93.

Bazant, Z.P., "Endochronic and Classical Theories of Plasticity in Finite Element Analysis," Finite Elements in Nonlinear Mechanics, Proceedings of the International Conference on Finite Elements in Nonlinear Solid and Structural Mechanics, Geilo, Norway, Vol. 1, 1977, pp. 151-165.

Bazant, Z.P., "Endochronic Inelasticity and Incremental Plasticity," International Journal of Solids and Structures, Vol. 14, No. 9, 1978, pp. 691-714.

Bazant, Z.P., "Physical Models for Steel Corrosion in Concrete Sea Structures - Theory," Journal of the Structural Division, ASCE, Vol. 105, No. 6, 1979a, pp. 1137-1153.

Bazant, Z.P., "Physical Models for Steel Corrosion in Concrete Sea Structures - Applications," Journal of the Structural Division, ASCE, Vol. 105, No. 6, 1979b, pp. 1155-1166.

Bazant, Z.P., Ansal, A.M., and Krizek, R.J., "Endochronic Models for Soils," Proceedings of the International Symposium on Soil Mechanics-Transient and Cyclic Loads, Eds. Pande, G.N., and Zienkiewicz, O.C., John Wiley & Sons Ltd., New York, 1982, pp. 419-438.

Bazant, Z.P., and Bhat, P.D., "Endochronic Theory of Inelasticity and Failure of Concrete," Journal of the Engineering Mechanics Division, ASCE, Vol. 102, No. 4, 1976, pp. 701-722.

Bazant, Z.P., and Bhat, P.D., "Prediction of Hysteresis of Reinforced Concrete Members," Journal of the Structural Division, ASCE, Vol. 103, No. 1, 1977, pp. 153-167.

Bazant, Z.P., and Krizek, R.J., "Endochronic Constitutive Model for Liquefaction of Sand," Journal of the Engineering Mechanics Division, ASCE, Vol. 102, No. 2, 1976, pp. 225-238.

Bazant, Z.P., Krizek, R.J., and Shieh, C.L., "Hysteretic Endochronic Theory for Sand," Journal of the Engineering Mechanics Division, ASCE, Vol. 109, No. 4, 1983, pp. 1073-1095.

Bazant, Z.P., and Shieh, C.L., "Endochronic Model for Nonlinear Triaxial Behavior of Concrete," Nuclear Engineering and Design, Vol. 47, 1978, pp. 305-315.

Beeby, A.W., "Corrosion of Reinforcing Steel in Concrete and its Relation to Cracking," The Structural Engineer, Vol. 56, No.3, 1978, pp. 77-81.

Blouin, S.E., Chamberlain, E.J., Sellman, P.V., and Garfield, D.E., "Penetration Tests in Subsea Permafrost, Prudhoe Bay, Alaska," CRREL (Cold Regions Research Engineering Laboratory) Report 79-7, Hanover, New Hampshire, May 1979.

Burns, N.H., and Siess, C.P., "Load-Deformation Characteristics of Beam-Column Connections in Reinforced Concrete," Structural Research Series No. 234, Civil Engineering Studies, University of Illinois, Urbana, January, 1962.

Chen, W.F., "Plasticity in Reinforced Concrete," McGraw-Hill Book Company, New York, 1982.

Chen, W.F., and Ting, E.C., "Constitutive Models for Concrete Structures," Journal of the Engineering Mechanics Division, ASCE, Vol. 106, No. 1, 1980, pp. 1-19.

Darwin, D., and Pecknold, D.A., "Nonlinear-Biaxial Law for Concrete," Journal of the Engineering Mechanics Division, ASCE, Vol. 103, No. 2, 1977, pp. 229-241.

Gerstle, K.H., "Simple Formulation of Biaxial Concrete Behavior," American Concrete Institute Journal, Vol. 78, No. 1, 1981a, pp. 62-68.

Gerstle, K.H., "Simple Formulation of Triaxial Concrete Behavior," American Concrete Institute Journal, Vol. 78, No. 5, 1981b, pp. 382-387.

Gjorv, O.E., "Long Time Durability of Concrete in Sea Water," American Concrete Institute Journal, Vol. 68, No. 1, 1971, pp. 60-67.

Gopal, K.R., and Reddy, D.V., "Endochronic Constitutive Modeling of Frozen Soil," ARCTIC '85:Proceedings of the Civil Engineering in the Arctic Offshore, San Francisco, California, 1985, pp. 584-592.

Haldar, A.K., Reddy, D.V., and Arockiasamy, M., "Offshore Platform Shakedown Analysis," Proceedings of the International Conference on the Behavior of Offshore Structures(BOSS), Boston, Massachusetts, 1982, pp. 313-333.

Hannant, D.J., "Fiber Cements and Fiber Concretes," John Wiley, London, England, 1978.

Hansen, T.C., "Influence of Aggregate and Voids on Modulus of Elasticity of Concrete, Cement Mortar and Cement Paste," American Concrete Institute Journal, Vol. 62, No. 2, 1965, pp. 193-216.

Henager, C.H., and Doherty, T.J., "Analysis of Reinforced Concrete Beams," Journal of the Structural Division, ASCE, Vol. 102, No. 1, 1976, pp. 177-188.

Hillerborg, A., Modeer, M., and Petersson, P.E., "Analysis of Crack Formation and Crack Growth in Concrete by Means of Fracture Mechanics and Finite Elements," Cement and Concrete Research, Vol. 6, 1976, pp. 773-782.

Hoff, G.C., Fontenot, C.M., and Tom, J.G., "Selected Bibliography on Fiber-Reinforced Cement and Concrete," Miscellaneous Paper C-76-6, U.S. Army Waterways Experiment Station, Vicksburg, Mississipi, 1976.

Hoff, G.C., "Selected Bibliography on Fiber-Reinforced Cement and Concrete," Supplement No. 1 for Paper C-76-6, U.S. Army Waterways Experiment Station, Vicksburg, Mississipi, 1977.

Hoff, G.C., "Selected Bibliography on Fiber-Reinforced Cement and Concrete," Supplement No. 2 for Paper C-76-6, U.S. Army Waterways Experiment Station, Vicksburg, Mississipi, 1979.

Houston, A., and Ferguson, P.M., "Corrosion of Reinforcing Steel Embedded Structural Concrete," Research Report 112-1-F, Center for Highway Research, University of Texas, Austin, Texas, 1972.

Hughes, B.P., and Fattuhi, N.I., "Load-deflection Curves for Fiber Reinforced Concrete Beams in Flexure," Magazine of Concrete Research, Vol. 29, No. 101, 1977a, pp. 199-206.

Hughes, B.P., and Fattuhi, N.I., "Modeling the Flexural Strength of Steel and Polypropylene Fiber-Reinforced Cement Based Beams," Journal of Composites, Vol. 8, No. 1, 1977b, pp. 57-61.

Hughes, B.P., and Fattuhi, N.I., "Stress-Strain Curves for Fiber Reinforced Concrete in Compression," Cement and Concrete Research, Vol. 7, 1977c, pp. 173-184.

Jain, S.K., "On the Thermodynamic Derivation of the Constitutive Equations of the Endochronic Theory of Viscoplasticity," Engineering Publications, Blacksburg, Virginia, 1982.

Johnston, C.D., "Steel Fiber Reinforced and Plain Concrete: Factors Influencing the Flexural Strength Measurements," American Concrete Institute Journal, Vol. 79, No. 2, 1982, pp. 131-138.

Keer, J.G., "Behavior of Cracked Fiber Composites Under Cyclic Loading," International Journal of Cement Composites, Vol. 3, No. 2, 1981, pp. 179-186.

Kormeling, H.A., Reinhardt, H.W., and Shah, S.P., "Static and Fatigue Properties of Concrete Beams with Continuous Bars and with Fibers," American Concrete Institute Journal, Vol. 77, No. 1, 1980, pp. 36-43.

Kupfer, H.B., and Gerstle, K.H., "Behavior of Concrete under Biaxial Stress," Journal of the Engineering Mechanics Division, ASCE, Vol. 99, No. 4, 1973, pp. 853-866.

Ladanyi, B., "Mechanical Behavior of Frozen Soils," Mechanics of Structured Media, Proceedings of the Third International Symposium on the Mechanical Behavior of Structured Media, Ottawa, Canada, 1981, Part-B, pp. 205-245.

Lin, H.C., and Wu, H.C., "On the Rate-Dependent Endochronic Theory of Viscoplasticity and its Application to Plastic Wave Propogation," International Journal of Solids and Structures, Vol. 19, No. 7, 1983, pp. 587-599.

Liu, T.C.Y., Nilson, A.H., and Slate, F.O., "Stress-Strain Response and Fracture of Concrete in Uniaxial and Biaxial Compression," American Concrete Institute Journal, Vol. 69, No. 5, 1972, pp. 291-295.

Mandel, J.A., and Pack, S.C., "Crack Growth in Fiber-Reinforced Materials," Journal of the Engineering Mechanics Division, ASCE, Vol. 108, No. 3, 1982, pp. 509-526.

Mather, B., "Concrete in Sea Water," Concrete International, Vol. 4, No. 3, 1982, pp. 28-34.

Matsuishi, M., and Iwata, S., "Probabilistic Strength of Steel Fiber Reinforced Concrete," Proceedings of the Third International Conference on the Behavior of Offshore Structures(BOSS), Boston, Massachusetts, Vol. 2, 1982, pp. 837-846.

McKee, D.C., "The Properties of an Expansive Cement Mortar Reinforced with Random Wire Fibers," Ph.D. Thesis, University of Illinois, Urbana, 1969.

Mindess, S., Lawrence, F.V., and Kesler, C.E., "The J-Integral as a Fracture Criterion for Fiber Reinforced Concrete," Cement and Concrete Research, Vol. 7, 1977, pp. 731-742.

Murray, D.W., "Octahedral Based Incremental Stress-Strain Matrices," Journal of the Engineering Mechanics Division, ASCE, Vol. 105, No. 4, 1979, pp. 501-513.

Naaman, A.E., Moavenzadeh, F., and McGarry, F.J., "Probabilistic Analysis of Fiber Reinforced Concrete," Journal of the Engineering Mechanics Division, ASCE, Vol. 100, No. 2, 1974, pp. 397-413.

Naaman, A.E., and Shah, S.P., "Pull-Out Mechanism in Steel Fiber Reinforced Concrete," Journal of the Structural Division, ASCE, Vol. 102, No. 8, 1976, pp. 1537-1548.

Nagaraj, T.S., and Dwarakanath, H.V., "Structural Response of Partially Fibrous Concrete Beams," Journal of the Structural Division, ASCE, Vol. 110, No. 11, 1984, pp. 2798-2812.

Ngo, D., and Scordelis, A.C., "Finite Element Analysis of Reinforced Concrete Beams," American Concrete Institute Journal, Vol. 64, No. 3, 1967, pp. 152-163.

Nilsson, S., "Impact Loading on Concrete Structures," Publication 79:1, Department of Structural Mechanics, Chalmers University of Technology, Goteberg, Sweden, 1979.

Nishibayashi, S., Yamura, K., and Inoue, S., "Durability of Concrete in Sea Water: Method of Accelerated Testing and Evaluation," Performance of Concrete in Marine Environment, American Concrete Institute, SP-65, Detroit, 1980, pp. 351-378.

O'Neil, E.F., "Study of Reinforced Concrete Beams Exposed to Marine Environment," Performance of Concrete in Marine Environment, American Concrete Institute, SP-65, Detroit, 1980, pp. 113-132.

Parameswaran, V.R., "Deformation Behavior and Strength of Frozen Sand," Canadian Geotechnical Journal, Vol. 17, No. 1, 1980, pp. 74-88.

Parameswaran, V.R., and Jones, S.J., "Triaxial Testing of Frozen Sand," Journal of Glaciology, Vol. 27, No. 95, 1981, pp. 147-156.

Parimi, S.R., and Rao, J.K.S., "On the Fracture Toughness of Fiber Reinforced Concrete," Proceedings of the Symposium on Fiber Reinforced Concrete, American Concrete Institute, Ottawa, Canada, 1973, pp. 79-92.

Park, R., Kent, D.C., and Sampson, R.A., "Reinforced Concrete Members with Cyclic Loading," Journal of the Structural Division, ASCE, Vol. 98, No. 7, 1972, pp. 1341-1359.

Phillips, D.V., and Zienkiewicz, O.C., "Finite Element Nonlinear Analysis of Concrete Structures," Proceedings of the Institution of Civil Engineers, Part-2, Vol. 61, No. 3, 1976, pp. 59-68.

Popovics, S., "A Review of Stress-Strain Relationships for Concrete," American Concrete Institute Journal, Vol. 67, No. 3, 1970, pp. 243-248.

Popovics, S., "A Numerical Approach to the Complete Stress-Strain Curve of Concrete," Cement and Concrete Research, Vol. 3, No. 5, 1973, pp. 583-599.

Rajagopalan, K., Parameswaran, V.S., and Rangaswamy, G.S., "Strength of Steel Fiber Reinforced Concrete Beams," Indian Concrete Journal, Vol. 48, No. 1, 1974, pp. 17-25.

Reddy, D.V., and Gopal, K.R., "Endochronic Constitutive Modeling of Fiber Reinforced Concrete," Proceedings of the International Conference on Computer Aided Analysis and Design of Concrete Structures, Split, Yugoslavia, September, 1984, Vol. 1, pp. 191-202.

Reddy, D.V., Gopal, K.R., Nomikos, G.G., and Thiel, D.T., "Strength and Durability of Fiber and Polymer-Modified Concrete for Marine Structural Applications," Research Report R/C-7, Florida Sea Grant College, Florida Atlantic Univeristy, Boca Raton, Florida, 1984.

Reddy, D.V., and Gopal, K.R., "Endochronic Constitutive Modeling of Marine Fiber Reinforced Concrete and Frozen Soil," Proceedings of the Fourth International Conference on Behavior of Offshore Structures (BOSS), Delft, The Netherlands, July, 1985.

Rider, R., and Heidersbach, R., "Degradation of Metal-Fiber Reinforced Concrete Exposed to a Marine Environment," Corrosion of Reinforcing Steel in Concrete, ASTM STP 713, American Society for Testing and Materials, Eds. Tonini, D.E., and Gaidis, J.M., 1980, pp. 75-92.

Rivlin, R.S., "Some Comments on the Endochronic Theory of Plasticity," International Journal of Solids and Structures, Vol. 17, 1981, pp. 231-248.

Romualdi, J.P., and Batson, G.B., "Mechanics of Crack Arrest in Concrete," Journal of the Engineering Mechanics Division, ASCE, Vol. 89, No. 3, 1963a, pp. 147-168.

Romualdi, J.P., and Batson, G.B., "Behavior of Reinforced Concrete Beams with Closely Spaced Reinforcement," American Concrete Institute Journal, Vol. 60, No. 6, 1963b, pp. 775-789.

Romualdi, J.P., and Mandel, J.A., "Tensile Strength of Concrete Affected by Uniformly Distributed and Closely Spaced Short Lengths of Wire Reinforcement," American Concrete Institute Journal, Vol. 61, No. 6, 1964, pp. 657-670.

Rudnicki, J.W., and Rice, J.R., "Conditions for the Localization of Deformation in Pressure Sensitive Dilatant Materials," Journal of the Mechanics and Physics of Solids, Vol. 23, 1975, pp. 371-394.

Sandler, I.S., "On the Uniqueness and Stability of Endochronic Theories of Material Behavior," Journal of the Applied Mechanics, ASME, Vol. 45, No. 2, 1978, pp. 263-266.

Sargin, M., "Stress-Strain Relationship for Concrete and the Analysis of Structural Concrete Sections," Study No. 4, Solid Mechanics Division, University of Waterloo, Waterloo, Ontario, Canada, 1971.

Schupak, M., "Design of Permanent Sea Water Structures to Prevent Deterioration," Concrete International, Vol. 4, No. 3, 1982, pp. 19-27.

Shah, S.P., Gokuz, U., and Ansari, F., "An Experimental Technique for Obtaining Complete Stress-Strain Curves for High Strength Concrete," American Society for Testing Materials, Vol. 3, No. 1, 1981, pp. 21-27.

Shah, S.P., and Rangan, B.V., "Properties of Fiber Reinforced Concrete," American Concrete Institute Journal, Vol. 68, No. 2, 1971, pp. 126-135.

Snyder, M.J., and Lankard, D.R., "Factors Affecting the Flexural Strength of Steel Fibrous Concrete," American Concrete Institute Journal, Vol. 69, No. 2, 1972, pp. 96-100.

Sorensen, S.I., Arnesen, A., and Bergan, P.G., "Nonlinear Finite Element Analysis of Reinforced Concrete Using Endochronic Theory," Proceedings of the International Conference on Finite Elements in Nonlinear Solids and Structural Mechanics, Geilo, Norway, 1977, pp. 167-189.

Stroeven, P., "Structural Modeling of Plain and Fiber Reinforced Concrete - A Morphological Approach to a Cracked Region," Journal of Composites, Vol. 13, No. 4, 1982, pp. 129-139.

Suidan, M., and Schnobrich, W.C., "Finite Element Analysis of Reinforced Concrete," Journal of the Structural Division, ASCE, Vol. 99, No. 10, 1973, pp. 2109-2122.

Swamy, R.N., "Fiber Reinforced Concrete: Mechanics, Properties and Applications," Indian Concrete Journal, Vol. 48, No. 1, 1974, pp. 7-16.

Swamy, R.N., and Mangat, P.S., "A Theory for the Flexural Strength of Steel Fiber Reinforced Concrete," Cement and Concrete Research, Vol. 4, 1974, pp. 313-325.

Swamy, R.N., Mangat, P.S., and Rao, C.V.S.K., "The Mechanics of Fiber Reinforcement of Cement Matrices," Proceedings of the International Symposium on Fiber Reinforced Concrete, Ottawa, Canada, 1973, pp. 1-28.

Tanigawa, Y., and Hatanaka, S., "Stress-Strain Relations of Steel Fiber Reinforced Concrete Under Repeated Compressive Load," Cement and Concrete Research, Vol. 13, 1983, pp. 801-808.

Taylor, H.P.J., and Sharp, J.V., "Fatigue on Offshore Concrete Structures," The Structural Engineer, Vol. 56, No. 3, 1978, pp. 69-76.

Tsai, S.W., "Structural Behavior of Composite Materials," NASA CR-31, National Aeronautics and Space Adminstration, Cleveland, Ohio, 1964.

Valanis, K.C., "A Theory of Viscoplasticity Without a Yield Surface - Theory and Application," Archives of Mechanics, Vol. 23, No. 4, 1971, pp. 517-551.

Valanis, K.C., "Fundamental Consequences of a New Intrinsic Time Measure - Plasticity as a Limit of the Endochronic Theory," Archives of Mechanics, Vol. 32, No. 1, 1980, pp. 171-191.

Valanis, K.C., "On the Substance of Rivlin's Remarks on the Endochronic Theory," International Journal of Solids and Structures, Vol. 17, 1981, pp. 249-265.

Valanis, K.C., and Lee, C.F., "Some Recent Developments of the Endochronic Theory with Applications," Nuclear Engineering and Design, Vol. 69, 1982, pp. 327-344.

Valanis, K.C., and Lee, C.F., "Endochronic Theory of Cyclic Plasticity with Applications," Journal of Applied Mechanics, ASME, Vol. 51, No. 2, 1984, pp. 367-374.

Valanis, K.C., and Read, H.E., "A New Endochronic Plasticity Model for Soils," Proceedings of the International Symposium on Soil Mechanics-Transient and Cyclic Loads, Eds. Pande, G.N., and Zienkiewicz, O.C., John Wiley and Sons Ltd., New York, 1982, pp. 375-417.

Valliappan, S., and Doolan, T.F., "Nonlinear Stress Analysis of Reinforced Concrete," Journal of the Structural Division, ASCE, Vol. 98, No. 4, 1972, pp. 885-898.

Velazco, G., Visalvanich, K., and Shah, S.P., "Fracture Behavior and Analysis of Fiber Reinforced Concrete Beams," Cement and Concrete Research, Vol. 10, 1980, pp. 41-51.

Wang, P.T., "Complete Stress-Strain Curve of Concrete its effects on the Ductility of Concrete," Ph.D. Thesis, University of Illinois, Chicago, 1977.

Wang, P.T., Shah, S.P., and Naaman, A.E., "Stress-Strain Curves of Normal and Light Weight Concrete in Compression," American Concrete Institute Journal, Vol. 75, No. 11, 1978a, pp. 603-611.

Wang, P.T., Shah, S.P., and Naaman, A.E., "High-Strength Concrete in Ultimate Strength Design," Journal of the Structural Division, ASCE, Vol. 104, No. 11, 1978b, pp. 1761-1773.

Wecharatana, M., and Shah, S.P., "A Model for Predicting Fracture Resistance of Fiber Reinforced Concrete," Cement and Concrete Research, Vol. 13, 1983, pp. 819-829.

Wu, H.C., and Sheu, J.C., "Endochronic Modeling of Shear Hysteresis of Sand," Journal of the Geotechnical Engineering Division, ASCE, Vol. 199, No. 12, 1983, pp. 1539-1550.

Wu, H.C., and Wang, T.P., "Endochronic Response of Sand to Static Loading," Journal of the Engineering Mechanics Division, ASCE, Vol. 109, No. 4, 1983, pp. 970-989.

Yuzugullu, O., and Schnobrich, W.C., "A Numerical Procedure for the Determination of the Behavior of a Shear Wall Frame System," American Concrete Institute Journal, Vol. 70, No. 7, 1973, pp. 474-479.

Zollo, R.F., "Extrusion of Steel Fiber Reinforced Concrete," American Concrete Institute Journal, Vol. 72, No. 12, 1975, pp. 675-677.

Zollo, R.F., "Fibrous Concrete Flexural Testing-Developing Standardized Techniques," American Concrete Institute Journal, Vol. 77, No. 5, 1980, pp. 363-368.

BIOGRAPHICAL SKETCH

The author was born at Kakinada in India on January 31, 1958. He received his B.Tech. degree in Civil Engineering with distinction from the Kakinada campus of Jawaharlal Nehru Technological University in May 1979 and the M.Tech. in Ocean Engineering from the Indian Institute of Technology at Madras in July 1981. He was awarded the Certificate of Academic Distinction for securing the first rank in the Ocean Engineering Class of 1979-81.

In August 1981 he was admitted to the Graduate College of Engineering at the University of Florida, Gainesville. The next four years were spent in working for a Doctoral degree during which time he served as a graduate research assistant in the Department of Coastal and Oceanographic Engineering. He was elected a member of the Florida Chapter of Tau Beta Pi Association in November 1982.

A part of his dissertation work was carried out at the Ocean Engineering Department, Florida Atlantic University, after his advisor moved there. He has published the following papers based on his dissertation work.

1) Gopal, K.R., Reddy, D.V., and Arockiasamy, M., "Endochronic Constitutive Modeling of Ice Behavior," Proceedings of the First Canadian Conference on Computer Methods in Offshore Engineering, Halifax, N.S., Canada, May, 1984.

2) Reddy, D.V., Gopal, K.R., Nomikos, G.G., and Thiel, D.T., "Strength and Durability of Fiber and Polymer Modified Concrete for Marine Structural Applications," Research Report R/C-7, Florida Sea Grant College, Florida Atlantic University, Boca Raton, Florida, 1984.

3) Reddy, D.V., and Gopal, K.R., "Endochronic Constitutive Modeling of Fiber Reinforced Concrete," Proceedings of the International Conference on Computer Aided Analysis and Design of Concrete Structures, Split, Yugoslavia, September, 1984, Vol. 1, pp. 191-202.

4) Gopal, K.R., and Reddy, D.V., "Endochronic Constitutive Modeling of Frozen Soil," ARCTIC '85: Proceedings of the Conference on the Civil Engineering in the Arctic Offshore, San Francisco, California, March, 1985, pp. 584-592.

5) Reddy, D.V., and Gopal, K.R., "Endochronic Constitutive Modeling of Marine Fiber Reinforced Concrete and Frozen Soil," Proceedings of the 4th International Conference on Behavior of Offshore Structures(BOSS), Delft, The Netherlands, July, 1985.

I certify that I have read this study and that in my opinion it conforms to acceptable standards of scholarly presentation and is fully adequate, in scope and quality, as a dissertation for the degree of Doctor of Philosophy.

H. Wang, Chairman
Professor of Coastal and
Oceanographic Engineering

I certify that I have read this study and that in my opinion it conforms to acceptable standards of scholarly presentation and is fully adequate, in scope and quality, as a dissertation for the degree of Doctor of Philosophy.

D.V. Reddy, Cochairman
Professor of Coastal and
Oceanographic Engineering

I certify that I have read this study and that in my opinion it conforms to acceptable standards of scholarly presentation and is fully adequate, in scope and quality, as a dissertation for the degree of Doctor of Philosophy.

M.A. Eisenberg
Professor of Engineering
Mechanics

I certify that I have read this study and that in my opinion it conforms to acceptable standards of scholarly presentation and is fully adequate, in scope and quality, as a dissertation for the degree of Doctor of Philosophy.

C.T. Sun
Professor of Engineering
Mechanics

I certify that I have read this study and that in my opinion it conforms to acceptable standards of scholarly presentation and is fully adequate, in scope and quality, as a dissertation for the degree of Doctor of Philosophy.

F.E. Fagundo
Assistant Professor of
Civil Engineering

This dissertation was submitted to the Graduate Faculty of the College of Engineering and to the Graduate School, and was accepted as partial fulfillment of the requirements for the degree of Doctor of Philophy.

August 1985

Dean, College of Engineering

Dean for Graduate Studies and
Research